



1 **Technical Note – AQMEII4 Activity 1: Evaluation of Wet and Dry Deposition Schemes as an Integral Part of**
2 **Regional-Scale Air Quality Models**

3 Stefano Galmarini^{1*}, Paul Makar², Olivia E. Clifton³, Christian Hogrefe^{4#}, Jesse O. Bash⁴, Roberto Bellasio⁵, Roberto
4 Bianconi⁵, Johannes Bieser⁶, Tim Butler⁷, Jason Ducker⁸, Johannes Flemming⁹, Alma Hodzic³, Christopher D. Holmes⁷,
5 Ioannis Kioutsioukis¹⁰, Richard Kranenburg¹¹, Aurelia Lupascu⁷, Juan Luis Perez-Camanyo¹², Jonathan Pleim⁴, Young-
6 Hee Ryu¹³, Roberto San Jose¹², Donna Schwede⁴, Sam Silva¹⁴, Marta Garcia Vivanco¹⁵, Ralf Wolke¹⁶

7

8 ¹Joint Research Center, European Commission, Ispra, Italy

9 ²Air Quality Modelling and Integration Section, Environment and Climate Change Canada, Toronto, Canada

10 ³National Center for Atmospheric Research, Boulder, CO, USA

11 ⁴Office of Research and Development, U.S. Environmental Protection Agency, Research Triangle Park, NC, USA

12 ⁵Enviroware srl, Concorezzo, MB, Italy

13 ⁶Institute of Coastal Research, Helmholtz-Zentrum Geesthacht, Germany

14 ⁷Institute for Advanced Sustainability Studies, Potsdam, Germany

15 ⁸Earth, Ocean and Atmospheric Science, Florida State University, Tallahassee, FL, USA

16 ⁹European Centre for Medium-Range Weather Forecasts, Reading, U.K.

17 ¹⁰Laboratory of Atmospheric Physics, Department of Physics, University of Patras, Greece

18 ¹¹Netherlands Organization for Applied Scientific Research (TNO), Utrecht, The Netherlands

19 ¹²Technical University of Madrid (UPM), Madrid, Spain

20 ¹³Pohang University of Science and Technology (POSTECH), Pohang, South Korea

21 ¹⁴Pacific Northwest National Laboratory, Richland, WA, USA

22 ¹⁵CIEMAT, Madrid, Spain

23 ¹⁶Leibniz Institute for Tropospheric Research, Leipzig, Germany

24

25

26 Corresponding authors: (*) Stefano.galmarini@ec.europa.eu, (#) Hogrefe.christian@epa.gov



27 **Abstract**

28 We present in this technical note the research protocol for Phase 4 of the Air Quality Model Evaluation International
29 Initiative (AQMEI4). This research initiative is divided in two activities, collectively having three goals: (i) to define
30 the current state of the science with respect to representations of wet and especially dry deposition in regional
31 models, (ii) to quantify the extent to which different dry deposition parameterizations influence retrospective air
32 pollutant concentration and flux predictions, and (iii) to identify, through the use of a common set of detailed
33 diagnostics, sensitivity simulations, model evaluation, and reducing input uncertainty, the specific causes for the
34 current range of these predictions. Activity 1 is dedicated to the diagnostic evaluation of wet and dry deposition
35 processes in regional air quality models (described in this paper), and Activity 2 to the evaluation of dry deposition
36 point models against ozone flux measurements at multiple towers with multiyear observations (in a subsequent
37 publication). The scope of these papers is to present the scientific protocols for AQMEI4, as well to summarize the
38 technical information associated with the different dry deposition approaches used by the participating research
39 groups of AQMEI4. In addition to describing all common aspects and data used for this multi-model evaluation
40 activity, most importantly, we present the strategy devised to allow a common process-level comparison of dry
41 deposition obtained from models using sometimes very different dry deposition schemes. The strategy is based on
42 adding detailed diagnostics to the algorithms used in the dry deposition modules of existing regional air quality
43 models, in particular archiving land use/land cover (LULC)-specific diagnostics and creating standardized LULC
44 categories to facilitate cross-comparison of LULC-specific dry deposition parameters and processes, as well as
45 archiving effective conductance and effective flux as means for comparing the relative influence of different
46 pathways towards the net or total dry deposition. This new approach, along with an analysis of precipitation and
47 wet deposition fields, will provide an unprecedented process-oriented comparison of deposition in regional air-
48 quality models. Examples of how specific dry deposition schemes used in participating models have been reduced
49 to the common set of comparable diagnostics defined for AQMEI4 are also presented.

50



51 **1. Introduction**

52 Since 2009, the Air Quality Model Evaluation International Initiative (AQMEII, Rao et al., 2011) has focused on
53 evaluating regional-scale air quality models used for research and regulatory applications. The goal of AQMEII is to
54 conduct coordinated research projects and model inter-comparisons to advance model evaluation practices and
55 inform model development. This initiative is promoted by the European Commission Joint Research Center, the U.S.
56 Environmental Protection Agency (EPA) and Environment and Climate Change Canada and involves the regional-
57 scale air quality research communities active in both North America and Europe.

58 AQMEII has been executed in phases that each focused on a critical aspect of modelling systems. The phases were
59 conducted as multi-model comparisons that were analyzed through the organization of common modelling activities
60 and supported by gathering specific monitoring data needed to evaluate model performance. Each of the phases
61 required developing innovative evaluation and data reconciliation techniques to provide scientific insight across
62 disparate modeling systems. AQMEII phase 1 provided the first detailed annual ensemble comparison of air-quality
63 model predictions for North America and Europe (Galmarini et al., 2012). AQMEII phase 2 examined the impacts of
64 feedbacks between air-quality and weather on forecasting skill and identified the key sources of uncertainty in
65 feedback model forecasts (Galmarini et al., 2015). AQMEII phase 3, in collaboration with the Task Force on
66 Hemispheric Transport of Air Pollution (TF HTAP) (<http://www.htap.org>), studied the effects of intercontinental
67 transport on regional air quality predictions (Galmarini et al., 2017). Details and findings of the past three phases of
68 AQMEII can be found in journal special issues dedicated to these activities (Galmarini et al., 2012, 2015, 2017). The
69 AQMEII initiative is based on the four pillars of model evaluation described by Dennis et al. (2010): operational,
70 diagnostic, dynamic, and probabilistic evaluation, which will be partly described hereinafter.

71 This fourth phase of AQMEII (AQMEII4), detailed in this special issue and introduced by a pair of technical notes,
72 focuses on the processes of wet and especially dry deposition, including the parameterized approaches used within
73 current air quality models, and how these approaches and the details of their implementation influence model
74 predictions and performance across multiple modelling systems. Deposition is critical to the lifecycle of a pollutant,
75 as it regulates the rate of pollutant removal from the atmosphere and determines the net flux of that pollutant to
76 the earth's surface. This latter point is particularly important when the pollutants have a known deleterious effect
77 on ecosystems (e.g. the deposition of acidifying compounds to aquatic ecosystems, or the dry deposition of ozone
78 on vegetation). By affecting the pollution remaining in the atmosphere, deposition estimates also modulate
79 predictions of ambient pollutant concentrations that affect human health through inhalation exposure.

80 Deposition has only been peripherally investigated in past phases of AQMEII. The operational evaluation of air
81 quality models, in which modelled concentrations are directly compared to monitoring network observations,
82 quantifies the extent to which an air quality model meets expected performance. However, operational evaluation
83 does not provide the process-level understanding of the extent to which the performance results from correct
84 representation of model physical and chemical processes. In this context, dry and wet deposition are key processes
85 within air quality models because they represent removal, which can affect the concentrations of key atmospheric



86 species. Several past AQMEII publications were dedicated specifically to wet and dry deposition (Vivanco et al. 2018,
87 Hogrefe et al. 2020, Solazzo et al. 2018). However, only wet deposition fluxes could be evaluated against
88 observational data in these papers. The causes of differences in model predictions for dry deposition were not
89 determined. Some of the studies performed within AQMEII also addressed dynamic evaluation (i.e. the performance
90 of a model in capturing changes in concentrations or deposition fluxes when subjected to variations in meteorology
91 or emissions). The effects of these variations on deposition were therefore investigated, but without analysis at the
92 process level on the extent to which the details of deposition algorithms influenced model performance.

93 Recent studies of dry deposition of ozone have been fueled by the need to quantify impacts on global-to-regional
94 water and carbon cycles (Lombardozzi et al., 2015; Oliver et al., 2018), vegetation damage including crop yields
95 (McGrath et al., 2015; Emberson et al., 2018; Schiferl and Heald, 2018; Hong et al., 2020), and ozone air pollution
96 (Andersson and Engardt, 2010; Silva and Heald, 2018; Baublitz et al., 2020). In particular, reduced stomatal dry
97 deposition of ozone during droughts may contribute to high ozone pollution episodes (Vautard et al., 2005; Solberg
98 et al., 2008; Emberson et al., 2013; Huang et al., 2016; Anav et al., 2018; Lin et al., 2020). Dry deposition of ozone
99 occurring through nonstomatal deposition pathways, on average 45% of the total (Clifton et al., 2020a), has also
100 been shown to be more variable and more important than predicted by current chemical transport models, with
101 implications for background and extreme ozone pollution (Clifton et al., 2017, 2020b). Previous intercomparisons at
102 the global scale suggest large differences in simulated ozone deposition velocities with implications for the simulated
103 tropospheric ozone budgets and the models' ability to quantitatively capture the drivers of recent trends and
104 interannual variability in observed ozone pollution (Hardacre et al., 2015; Wong et al., 2019). However, process-
105 oriented evaluation in regional-to-global models is missing, in large part because key process-oriented diagnostics
106 have not been archived and different land use / land cover (LULC) inputs across models have inhibited the systematic
107 elucidation of processes driving the noted differences (Hardacre et al., 2015; Clifton et al., 2020a). One way in which
108 discrepancies between observed and modelled deposition has been addressed is through model-measurement
109 fusion approaches (Schwede and Lear, 2014; Makar et al., 2018, Robichaud et al., 2019, Robichaud et al., 2020). Such
110 approaches could benefit from an improved characterization of process-level uncertainty in modeled dry deposition.

111 Despite the great advancements in regional-scale air quality modelling, the primary schemes used for dry and wet
112 deposition in today's models originated in the 1980's and 1990's. Moreover, while the role of deposition as a
113 persistent sink has been known for a long time (e.g. Chang et al., 1987; Irving and Smith, 1991; Borrell and Borrell,
114 2000), its relative importance in regulating trace species budgets has become more prominent in recent years as the
115 magnitude of the anthropogenic emission source term has generally decreased. The evaluation studies performed
116 within AQMEII (e.g., Solazzo et al. 2017; Hogrefe et al., 2018) and other recent work reaffirmed that deposition is a
117 process of paramount importance within an air quality model (e.g., Knote et al., 2015; Huang et al., 2016; Beddows
118 et al., 2017; Matichuk et al., 2017; Campbell et al., 2019; Sharma et al., 2020) with consequences of primary
119 relevance in a number of sectors (human health, agriculture, forestry, hydrology, soil management, ecosystems
120 management). Thus, there is renewed focus on better characterization of this term and its magnitude.



121 All the above points were the motivation to make use of the AQMEII community and evaluation infrastructure to
122 construct an AQMEII phase dedicated to deposition. This phase was designed to compare deposition predictions
123 from multiple regional models by isolating specific deposition pathways across multiple modelling systems and
124 across multiple LULC classification systems using common diagnostic tools. Analyzing dry deposition of gaseous
125 species, especially ozone and nitrogen species, is a particular focus, as is quantifying the range of model predictions
126 for acidifying wet and dry deposition. A process-level diagnostic intercomparison of particle dry deposition is not
127 conducted here due to the complexity added by model-to-model differences in the representation of aerosols (size
128 and composition) themselves. We also note that some previous work (e.g. Makar et al., 2018) suggests that the
129 impact of particle deposition on total nitrogen and sulphur deposition is relatively small, although particle deposition
130 is the main source of base cations transferred from the atmosphere to ecosystems. However, more recent work
131 (Saylor et al., 2019, Emerson et al., 2020) suggests that particle dry deposition algorithms used in current modelling
132 systems are highly uncertain, suggesting a need for performing further process-level diagnostic intercomparisons.

133 AQMEII4 has the following research goals:

- 134 • Quantify the performance and variability of dry and wet deposition fields simulated by multiple state-of-
135 the science regional air quality models.
- 136 • Document deposition schemes and key parameters used in these models in a framework that allows their
137 easy intercomparison.
- 138 • Identify and quantify the causes of differences in model-generated deposition fluxes by using detailed
139 ancillary diagnostic fields added to deposition algorithms and common LULC categories.
- 140 • Analyze dry deposition module performance with single-point model simulations driven by observation
141 data collected at towers with ozone flux measurements, and quantify the impacts of different conditions,
142 processes and parameters on simulated dry deposition (Activity 2; to be covered in a companion technical
143 note).
- 144 • Investigate methods for using simulated meteorological, concentration, and deposition fields from multiple
145 models in conjunction with available observations to estimate maps of total deposition and their
146 environmental impacts, including the prediction of exceedances of critical loads.

147

148 Most model dry deposition schemes are derived from Wesely (1989). However, their implementation in regional
149 and global models has considerable variation (a comparison with global models may be found in Hardacre et al.,
150 2015). Specifically, most schemes follow the parameterization structure used by Wesely (1989) but may differ in the
151 details of their representation of individual parameters and processes. This is discussed in more detail in Section 3.

152 In addition, dry deposition algorithms require, as a key input, information on LULC and vegetation. It is therefore
153 important to determine how the deposition modules themselves work, both as standalone physical descriptions,
154 and within a regional air quality model. AQMEII4 has been organized as two parallel activities to address the research
155 goals outlined above. AQMEII4 Activity 1 (introduced in this technical note) focuses on the detailed diagnostic



156 comparison of predictions of air quality model deposition fields, along with evaluation of model concentration and
157 wet deposition flux performance at routine monitoring stations in North America (NA) and Europe (EU). Activity 2
158 (introduced in a separate technical note) evaluates only the dry deposition schemes used in air quality models, and
159 other models used for impacts assessments, as zero-dimensional single-point models, driven by observed
160 meteorology, biophysics and ecosystem characteristics, at specific sites across the Northern Hemisphere where
161 ozone flux measurements have been collected continuously over at least a year, with many datasets spanning three
162 years or more. AQMEI4 will provide the most comprehensive analyses yet performed on dry deposition schemes,
163 since the schemes will be tested both within and independently from the air quality model, under controlled
164 conditions, and when subjected to variable meteorological and surface characteristic conditions. The single-point
165 modelling component allows a very detailed analysis of how ozone dry deposition is modeled; recent work
166 comparing 5 deposition algorithms at a single site (Wu et al., 2018) here has been extended to multiple sites,
167 additional deposition algorithms, and takes advantage of a new collection of ozone flux measurements at sites
168 around the Northern Hemisphere and new process-oriented diagnostics.

169 This technical note is the first of two which are designed to summarize all relevant information that constitute the
170 set up and organization of AQMEI4. The intent of these technical notes is to provide both the readers and authors
171 of this Special Issue with a common reference for the description of the AQMEI4 aims, scientific protocols, and
172 analysis approaches, the model reporting framework, the model input data and monitoring data used for model
173 evaluation, and descriptions of the model deposition algorithms themselves. By serving as common point of
174 reference for the individual studies undertaken through the AQMEI4 framework, these technical notes reduce the
175 need for repetition of background material by individual study papers which allows these papers to focus on specific
176 analyses and the presentation of the results of AQMEI4. They also allow the reader to access all relevant background
177 material in a single location rather than spread out over several papers. Because of this design, these technical notes
178 should not be viewed as stand-alone scientific papers as they do not contain any results, but rather as laying the
179 groundwork for subsequent scientific papers contributed by modeling groups to the AQMEI4 Special Issue. This first
180 technical note is dedicated to Activity 1 while the second is dedicated to Activity 2.

181

182 **2. AQMEI4 Activity 1 Description**

183 Activity 1 like the previous phases of AQMEI includes the evaluation of regional air quality model simulation on the
184 NA, EU, or both domains for at least a one-year period. Prior to describing the requested output that pertains strictly
185 to dry deposition, we briefly summarize in this section the modeling periods and domains, common inputs, and
186 standard concentration, meteorology, and wet deposition outputs for Activity 1.

187 **2.1 Modeling Periods and Domains**

188 For AQMEI4 Activity 1 the air quality community listed in Table 1 has been asked to perform two annual simulations
189 of the air quality over NA and/or EU.



190

Group/Institution	Modeling System	Model Domains
Leibniz Institute for Tropospheric Research (TROPOS), Germany	COSMO / MUSCAT	EU
Environment and Climate Change Canada (ECCC), Canada	GEM / MACH (3 different model configurations)	NA
Technical University of Madrid (UPM), Spain	WRF-Chem	EU and NA
Netherlands Organization for Applied Scientific Research (TNO), The Netherlands	LOTOS / EUROS	EU
Institute for Advanced Sustainability Studies (IASS), Germany	WRF-Chem	EU and NA
US Environmental Protection Agency, USA	WRF / CMAQ (2 different model configurations)	NA
Helmholtz-Zentrum Geesthacht, Germany	COSMO-CLM / CMAQ	EU and NA
National Center for Atmospheric Research (NCAR), USA	WRF-Chem	NA
University of Hertfordshire, United Kingdom	WRF / CMAQ	EU
Research Centre for Energy, Environment and Technology (CIEMAT), Spain	ECMWF/IFS / CHIMERE	EU

191

192 **Table 1. Participating institutes, models names and cases simulated**

193

194 Specifically, the years of interest in AQMEII4 are: North America - 2010 and 2016; Europe - 2009 and 2010. The NA
195 years were selected due their past use in policy-relevant emissions scenario simulation, with changes in emission
196 policies that may affect the deposition. In the case of Europe, the years illustrated a marked difference in
197 meteorological signatures between the two years, hence providing a gauge of the impact of meteorological
198 variability on deposition. Modeling multiple years also allows the investigation of the variability of impacts of
199 emission policies and weather conditions on deposition patterns.

200 All modeling groups carried out simulations on their own grid projections. These “native grid” simulations were
201 interpolated to a common 0.125° x 0.125° latitude-longitude grid over each continent to allow direct comparison of
202 gridded model data:

203 NA: 130°W <-> 59.5°W, 23.5°N <-> 58.5°N,

204 EU: 30 W <-> 60°E, 25°N <-> 70°N



205 Modeling groups are expected to perform their simulations on a grid with comparable-to-higher horizontal
206 resolution as these reported grids. The interpolation of model results from the native modeling grid to the common
207 analysis grid was recommended to use a mass conserving method for concentrations and fluxes and the nearest
208 neighbor method for diagnostic variables.

209 **2.2. Model Inputs Shared By All Participants**

210 Air-quality models require input fields for meteorology, emissions and chemical boundary conditions; differences in
211 each of these fields lead to differences in model results. All AQMEII exercises have considered the driving
212 meteorology to be an integral part of each participating model (for on-line models, such as studied under AQMEII-2
213 chemistry and meteorology are inseparable, since both are included in the same modelling platform) and have
214 therefore not attempted to harmonize meteorological fields across participants. However, variations caused by
215 different emissions and chemical boundary conditions are removed in all AQMEII phases by requiring all participating
216 models to use a common set of emissions and lateral chemical boundary conditions (Galmarini et al., 2012, 2015,
217 2017). Note that due to their dependence on model-specific LULC and meteorology, biogenic emissions are not
218 prescribed and are generated by each group. For AQMEII4, the common model inputs were prepared as follows:

219 *2.2.1 Anthropogenic Emissions*

220 Emissions for anthropogenic sources over NA were prepared from U.S., Canadian, and Mexican inventory data using
221 the emissions processing approach developed for U.S. EPA “emission modeling platforms” (EMP). An EMP includes
222 not only the underlying point source, county or province level inventory data but also controls the temporal and
223 spatial allocation and chemical speciation of these inventories. For 2010, the processing was based on the “2011v6.3
224 EMP” (<https://www.epa.gov/air-emissions-modeling/2011-version-63-platform>). Year specific adjustments for 2010
225 were made to the EMP for several sectors (e.g. electric generating units, mobile sources, and residential wood
226 combustion) and Canadian emissions were based on a 2010 inventory rather than the 2013 inventory projected to
227 2011 used in the EMP. For 2016, the processing was based on the “2016beta EMP” (<https://www.epa.gov/air-emissions-modeling/2016v72-beta-and-regional-haze-platform>) which is documented at
228 <http://views.cira.colostate.edu/wiki/wiki/10197>. These EMP were used by the US EPA to generate 8 different hourly
229 speciated files for each day in 2010 (1 gridded file with low-level emissions and files with elevated sources from 7
230 different sectors) and 9 different hourly speciated files for each day in 2016 (1 gridded file with low-level emissions
231 and files with elevated sources from 8 different sectors) which were then shared with all participants. Speciation
232 was performed for both the CB6R3 and SAPRC07 mechanism to provide flexibility to participants to map emissions
233 to the chemical mechanism used in their model. The same data were used by Environment and Climate Change
234 Canada to generate day-specific emissions for the GEM-MACH air-quality model, for the ADOMII mechanism used
235 within that model. Annual gridded anthropogenic emissions using the Standard Nomenclature for Air Pollution
236 (SNAP) sector classification scheme were prepared over EU by TNO for 2009 and 2010 as part of the MACC-III project
237 (Kuenen et al., 2015) and were provided to EU modeling groups along with reference temporal allocation and
238 speciation profiles. If necessary, EU modeling groups used other emission datasets available to them to fill in
239



240 emissions near the edges of their modeling domains if their modeling domains extended beyond the are covered by
241 the MACC-III emissions provided by TNO.

242 *2.2.2 Forest Fire Emissions*

243 The forest fire emissions over NA for 2010 were a combination of emissions over the U.S. included in the “2011v6.3”
244 EMP and emissions over Canada provided by Environment and Climate Change Canada (ECCC) while 2016 forest fire
245 emissions over both the U.S. and Canada were obtained from the “2016 beta” EMP. Data distributed to modeling
246 groups included both the mass of emissions of Criteria Air Contaminants (speciated into the gases of the gas-phase
247 chemistry mechanisms noted above) and the parameters necessary to compute plume rise using a prescribed plume
248 rise algorithm based on the large stack plume rise formula of Briggs (Briggs, 1971, 1972). While different modelling
249 platforms often have their own approaches for estimating forest fire emissions, particularly in an operational
250 context, as was the case for anthropogenic emissions, this unified approach was adopted in order to reduce the
251 variability in model performance associated with emissions inputs. Forest fire emissions for 2009 and 2010 over EU
252 were provided by the Finnish Meteorological Institute and were developed using the IS4FIRESv2 methodology
253 described in Soares et al. (2015). These emissions were vertically allocated to eight layers with heights ranging from
254 50m to 6200m, with individual groups re-allocating the resulting mass to their own vertical discretization.

255 *2.2.3 NO emissions from lightning*

256 Although previous phases of AQMEII did not consider NO emissions from lightning, these emissions were included
257 in the current phase due to their impact on nitrogen deposition fluxes. To provide a unified forcing from this source
258 across all models, the emissions were based on the GEIA monthly climatology (Price et al., 1997) rather than in-line
259 parameterizations based on meteorological fields implemented in some but not all participating models. Although
260 using climatological lightning does not capture the linkage between modeled meteorology and NO emission from
261 lightning, this approach ensures that the bulk effects are included in all modeling systems and streamlines the
262 interpretation of the modeling results by removing a potential difference in emissions input. The monthly
263 climatological values were allocated diurnally based on Table 2 in Blakeslee et al. (2014) and distributed to
264 participating groups as 2-dimensional files. Groups were then asked to allocate these emissions to their specific
265 vertical grid based on Table 2 of Ott et al. (2010), using the tropical profiles for land and water (or an average of the
266 two) for grid cells with latitudes below 23.5N, the subtropical profile for grid cells with latitudes between 23.5°N and
267 40°N, and the midlatitude profile for grid cells with latitudes > 40°N.

268 *2.2.4 Chemical boundary conditions*

269 Concentrations of the 33 longer-lived trace gas and aerosol species listed in Table 2 were provided by the European
270 Centre for Medium-Range Weather Forecasts (ECMWF) for the two continents and for the modeled time periods so
271 that participants could prepare initial and boundary conditions for their regional-scale modeling domains. The
272 concentration fields were based on the Copernicus Atmospheric Monitoring Service (CAMS) EAC4 reanalysis product
273 (Inness et al., 2019) and were provided every 3 hours on a 0.75° x 0.75° grid with 54 vertical levels from the surface
274 to 2 hPa. The vertical grid structure varied in both resolution and vertical extent across models and individual



275 participants were responsible for interpolating the CAMS fields to their horizontal and vertical grid structure. The
 276 CAMS species were matched by participants to their own internal model speciation (and, in the case of the
 277 particulate matter emissions, to the particle size distribution of their own models).

Trace Gas Species	Aerosol Species	
O ₃ (ozone)	Sea Salt Aerosol @80% relative humidity (wet radii 0.03 - 0.5 μm)*	
CO (carbon monoxide)	Sea Salt Aerosol @80% relative humidity (wet radii 0.5 - 5 μm)*	
NO (nitrogen monoxide; nitric oxide)	Sea Salt Aerosol @80% relative humidity (wet radii 5 - 20 μm)*	
NO ₂ (nitrogen dioxide)	Dust Aerosol @0% relative humidity (dry radii 0.03 - 0.55 μm)	
PAN (peroxyacetyl nitrate)	Dust Aerosol @0% relative humidity (dry radii 0.55 - 0.9 μm)	
HNO ₃ (nitric acid)	Dust Aerosol @0% relative humidity (dry radii 0.9 - 20 μm)	
CH ₂ O (formaldehyde)	Hydrophobic Organic Matter Aerosol @0% relative humidity	
SO ₂ (sulfur dioxide)	Hydrophilic Organic Matter Aerosol @0% relative humidity	
H ₂ O ₂ (hydrogen peroxide)	Hydrophobic Black Carbon Aerosol @0% relative humidity	
CH ₃ COCH ₃ (acetone)	Hydrophilic Black Carbon Aerosol @0% relative humidity	
C ₂ H ₆ (ethane)	Sulphate Aerosol @0% relative humidity	
PAR (paraffins)		
CH ₃ OH (methanol)		
C ₃ H ₈ (propane)		
C ₂ H ₅ OH (ethanol)		
C ₂ H ₄ (ethene)		
ALD2 (aldehydes)		
OLE (olefins)		
C ₅ H ₈ (isoprene)		
HCOOH (formic acid)		
CH ₃ OOH (methylperoxide)		
ONIT (organic nitrates)		
*based on guidance from ECMWF, participants were advised to transform the provided values back to dry matter by applying a reduction factor of 4.3 for the mass mixing ratios and a reduction factor of 1.99 for the radii of the sea salt bin limits		

278

279 **Table 2. Variables from the CAMS EAC4 reanalysis provided for the generation of initial and boundary conditions.**

280 **2.3 Standard Model Outputs**

281 We distinguish here between model output similar in scope and intent to previous ensemble model comparisons in
 282 past phases of AQMEII (i.e., “standard model outputs”), and the detailed diagnostic outputs reported under
 283 AQMEII4. The standard output requested from all participating models comes in two major forms: as hourly gridded



284 surface concentrations and meteorological variables on the common grids described earlier, and as model values
285 extracted at monitoring network station locations. Tables A1 – A3 of Appendix A list the variables requested for gas
286 and particle phase species, meteorology, and grid scale deposition fluxes. The meteorological variables have been
287 extended considerably compared to past phases of AQMEII, to include more parameters that describe the planetary
288 boundary layer. The gridded fields of integrated emissions were also requested as output, to be used to check that
289 the right amounts of masses were inputted into the models.

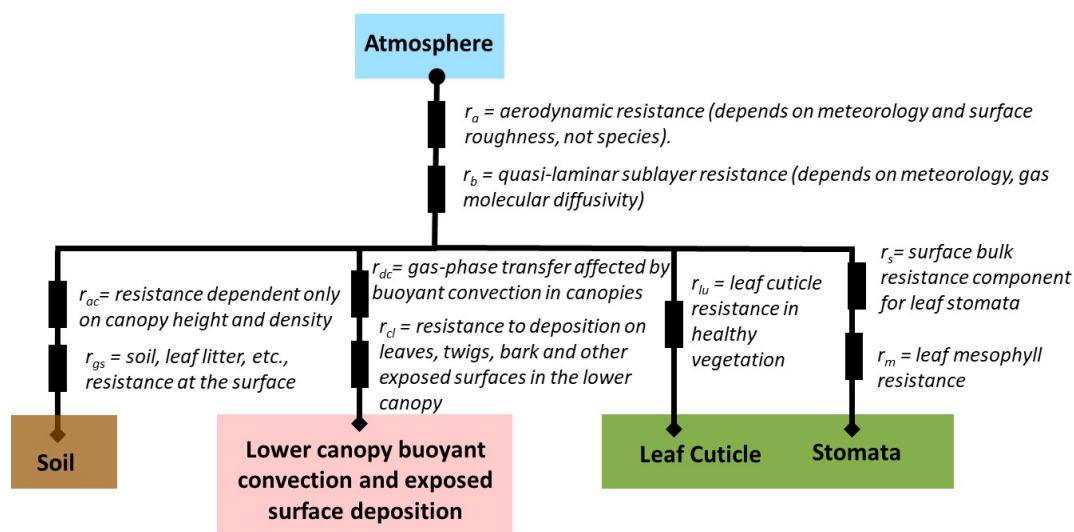
290 A list of all available surface monitoring locations in both continents for concentrations of gas- and particle-phase
291 species, precipitation chemistry, and meteorology was distributed to the AQMEII4 participants who are expected to
292 produce model results for all species presented in Appendix A for the grid location closest to the monitor or
293 interpolated to the monitoring. In particular, we note that the analysis of wet deposition in AQMEII4 will rely on the
294 precipitation and wet deposition flux variables listed in Table A3. In addition, the locations where vertical profiles
295 of ozone are routinely measured in NA and EU are also provided and modelling groups were expected to produce
296 the ozone vertical profiles at those spots. For more information on the routine monitoring networks used in AQMEII
297 please refer to Galmarini et al. (2012, 2015, 2017).

298

299 **3. Strategy For The Diagnostic Intercomparison Of Dry Deposition From Different Grid-Based Models**

300 Analysis of dry deposition is the focus of AQMEII4. In particular, AQMEII4 intends to go beyond an operational
301 evaluation of ambient concentrations and comparison of total deposition across models because this approach does
302 not provide enough information to determine the causes of different deposition totals among regional models. The
303 novelty of AQMEII4 is that we request additional and very detailed diagnostic-evaluation outputs related to dry
304 depositional from all of the models. With these very detailed outputs, we can compare the important elements of
305 the model machinery and understand model differences.

306 Many regional models use the Wesely (1989) dry deposition scheme, but several variants have been developed and
307 implemented with different levels of sophistication. Dry deposition schemes are mostly resistance frameworks – by
308 framework, we mean the structure of the scheme with respect to how processes relate to one another – and all of
309 the regional models in AQMEII4 use resistance frameworks for dry deposition. Resistance frameworks are based on
310 the representation of series and parallel resistors in electrical circuits. Differences in resistance frameworks across
311 regional models imply that comparing a given process among the regional models is not straightforward. Thus,
312 diagnostic variables that account for differences in resistance frameworks need to be reported. Below, we present
313 the strategy devised to reduce any dry deposition scheme to the essential set of comparable variables regardless of
314 the differences in the frameworks of the schemes that generated them.



315

316 **Figure 1. Schematic of the resistance framework for gas-phase dry deposition for the Wesely (1989) scheme.**
 317 **Circles and diamonds show where ozone concentration is needed as input for a given framework. At the diamonds,**
 318 **the ozone concentration is assumed to be zero. Rectangles indicate resistances.**

319

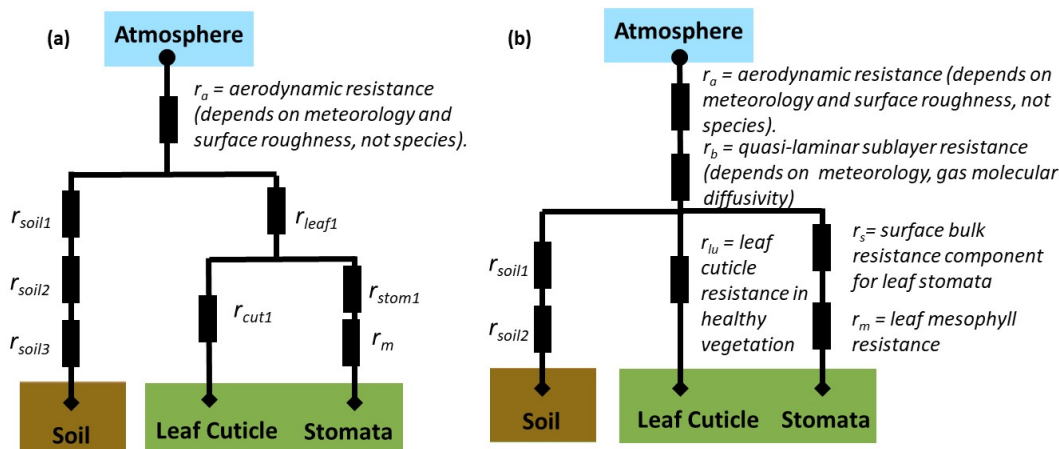
320 We start with a description of the Wesely (1989) resistance framework, one of the earliest literature examples of a
 321 resistance framework for dry deposition and arguably the most popular dry deposition scheme, and follow with both
 322 generic and specific examples of other resistance frameworks as a guide to the AQMEI4 output protocol. The
 323 components of the deposition velocity are process-based resistances (units s cm^{-1}) that impede the transfer of mass
 324 to a variety of surfaces. Resistances are added in series for processes operating on the same depositional pathway,
 325 and in parallel when multiple surfaces for dry deposition exist. In the original Wesely (1989) scheme, four deposition
 326 pathways were used: soil, “lower canopy and exposed surfaces”, leaf cuticles, and plant stomata. Gases are first
 327 impeded by an aerodynamic resistance to deposition (r_a), second impeded by a quasi-laminar sublayer resistance
 328 (r_b), and third impeded by a bulk surface resistance term (r_c) composed of a parallel summation of the resistances
 329 associated with each pathway. The three impedances to deposition are added into a total resistance, the inverse of
 330 which is the deposition velocity of the gas (units cm s^{-1}):

$$331 \quad v_d = (r_a + r_b + r_c)^{-1} \quad (1)$$

332 The bulk surface resistance (r_c) in Wesely (1989) follows:

$$333 \quad r_c = \left((r_s + r_m)^{-1} + (r_{lu})^{-1} + (r_{dc} + r_{cl})^{-1} + (r_{ac} + r_{gs})^{-1} \right)^{-1} \quad (2)$$

334 The component resistances used in r_c are defined in Figure 1, which is a schematic of the Wesely (1989) resistance
 335 framework.



336

337 **Figure 2. Two generic deposition resistance examples.**

338 Work subsequent to Wesely (1989) also uses the resistance approach, but sometimes with considerable variation in
 339 the resistance framework, the number of surfaces to which dry deposition occurs, and/or the processes represented
 340 by individual resistances. Schematics of resistance frameworks as two generic examples are shown in Figure 2. In
 341 these examples, the Wesely (1989) deposition pathway for “lower canopy buoyancy and exposed surfaces”
 342 deposition is not included. The example of Figure 2(a) also lacks a quasi-laminar sublayer resistance r_b applied across
 343 all surface types. Instead, surface-specific quasi-laminar sublayer resistances are used: r_{soil2} for soil and r_{leaf1} for
 344 leaves. The examples in Figure 2 demonstrate two ways in which the resistance framework has been adapted from
 345 Wesely (1989). In general, the diversity in resistance frameworks across models complicates model intercomparison
 346 of individual resistances.

347

348 When there are differences in resistance frameworks across models, the deposition pathways may be compared
 349 across models using a construct we will refer to here as *effective conductance* (Paulot et al., 2018; Clifton et al.,
 350 2020b). While generally a conductance is simply the inverse of a resistance, an *effective* conductance is the
 351 contribution of a given depositional pathway to the deposition velocity, expressed in the same units as the
 352 deposition velocity. The sum of the effective conductances for all deposition pathways is the deposition velocity.
 353 The effective conductances of the soil (E_{SOIL}), lower canopy (E_{LCAN}), cuticle (E_{CUT}) and stomata (E_{STOM}) branches
 354 specifically for Wesely (1989) are given by¹:

355

$$E_{SOIL} = \left(\frac{(r_{ac} + r_{gs})^{-1}}{(r_s + r_m)^{-1} + (r_{lv})^{-1} + (r_{dc} + r_{cl})^{-1} + (r_{ac} + r_{gs})^{-1}} \right) v_d \quad (3)$$

¹ Note that the depositing gases in each pathway are influenced by r_a and r_b prior to encountering the different resistances that make up r_c , and this is why v_d , which includes the influence of r_a and r_b , is scaled by the fraction of the inverse of r_c occurring through a given pathway. Some models include surface-specific quasi-laminar sublayer resistances; when this is the case, these terms appear in the pathway-specific fractions of the total uptake terms.



$$356 \quad E_{LCAN} = \left(\frac{(r_{dc}+r_{cl})^{-1}}{(r_s+r_m)^{-1}+(r_{lu})^{-1}+(r_{dc}+r_{cl})^{-1}+(r_{ac}+r_{gs})^{-1}} \right) v_d \quad (4)$$

$$357 \quad E_{CUT} = \left(\frac{(r_{lu})^{-1}}{(r_s+r_m)^{-1}+(r_{lu})^{-1}+(r_{dc}+r_{cl})^{-1}+(r_{ac}+r_{gs})^{-1}} \right) v_d \quad (5)$$

$$358 \quad E_{STOM} = \left(\frac{(r_s+r_m)^{-1}}{(r_s+r_m)^{-1}+(r_{lu})^{-1}+(r_{dc}+r_{cl})^{-1}+(r_{ac}+r_{gs})^{-1}} \right) v_d \quad (6)$$

359 The denominator in each of equations (3) to (6) is the inverse of the bulk surface resistance r_c and the numerators
360 are the inverses of the resistances associated with each pathway in r_c . We emphasize that the calculation of the
361 effective conductances depends on the resistance framework used; equations (3) to (6) are specific to Wesely (1989)
362 and require modification for other resistance frameworks, and we provide examples of formulae for these terms for
363 other frameworks, in Section 4.1, and Appendix B. Calculation of the effective conductances requires either
364 archiving all component resistances in a given framework and subsequent post-processing, or their online
365 calculation.

366 For any given model, effective conductances are an invaluable tool for determining the extent to which each
367 pathway impacts dry deposition velocity, and which deposition pathways drive spatiotemporal variability in dry
368 deposition velocity. Key for AQMEII4, the effective conductances allow a cross-comparison of the main deposition
369 pathways across different resistance frameworks. The primary terms of comparison for dry deposition schemes in
370 AQMEII4 are thus the effective conductances. In addition, given that many models' resistance frameworks follow
371 Wesely (1989), we also request those individual resistance terms held in common by most models, to allow exact
372 comparisons of individual processes which may influence or control a given pathway. These resistances include:

- 373 (1) A term for the aerodynamic resistance, r_a .
- 374 (2) A term for the bulk resistance to deposition associated with surfaces r_c .
- 375 (3) A term or series addition set of terms describing the stomatal resistance, r_s .
- 376 (4) A term or series addition set of terms describing the mesophyll resistance r_m .
- 377 (5) A term or series addition set of terms describing the cuticle resistance, r_c .
- 378 (6) Terms to describe quasi-laminar sublayer resistance, r_b .
- 379 (7) A term to describe within-canopy buoyant convection, r_{dc} .

380 With regards to (6), the implementation of quasi-laminar sublayer resistance (r_b in Wesely (1989)) tends to differ
381 among models. Some models use the Wesely (1989) concept of a pathway-independent quasi-laminar sublayer
382 resistance. Others use quasi-laminar sublayer resistances as pathway-dependent (e.g. Fig. 2a, where the r_{soil2} and
383 r_{leaf1} represent quasi-laminar sublayer resistances for soil and leaf pathways, respectively). The quasi-laminar
384 sublayer resistance is thus reported in AQMEII4 for each pathway, with the models for which the term is independent
385 of pathway reporting the same value for each pathway. Pathway-dependent quasi-laminar sublayer resistances are
386 to be reported as "not present" only if the given pathway does not exist in the framework.

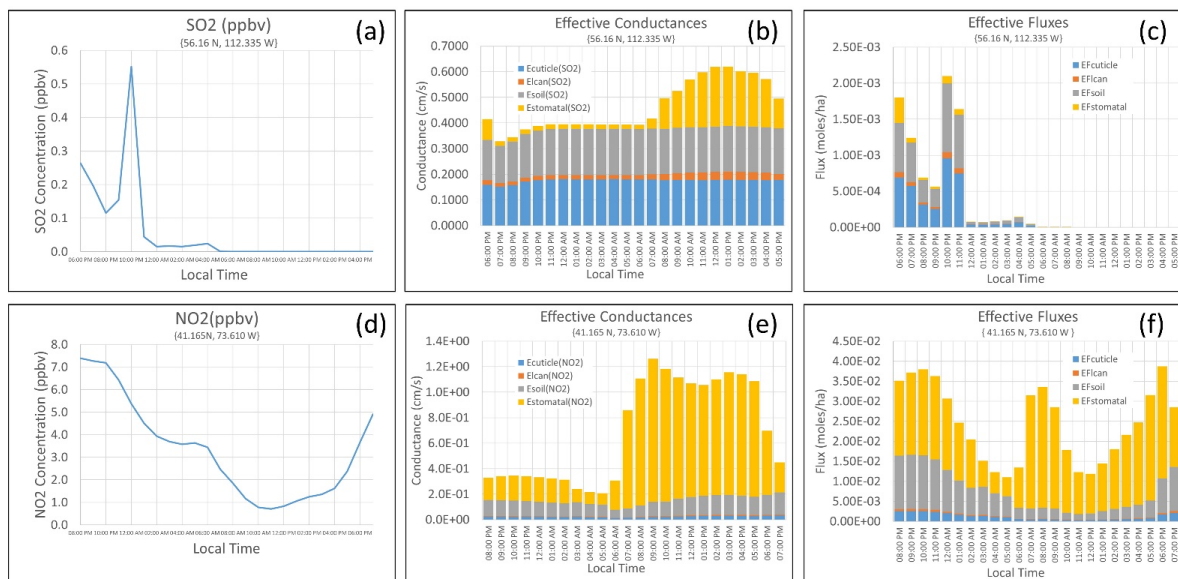


387 Note that models that include a single deposition pathway to soil that incorporates r_{dc} are requested to report that
388 pathway as “lower canopy” not “soil”. For example, the LOTOS-EUROS dry deposition scheme (Fig. B4) reports the
389 effective conductance calculated for the soil pathway as E_{LCAN} due to the presence of the in-canopy resistance term
390 in this pathway. In contrast, the CMAQ-M3DRY and CMAQ-STAGE dry deposition schemes (Figs. B2 and B3) have two
391 separate pathways for deposition to soil, one for vegetation-covered soil and one for bare soil. Due to the inclusion
392 of the in-canopy convective resistance in the computations for vegetation-covered soil, the effective conductance
393 for that pathway is reported as E_{LCAN} , while the effective conductance for the bare soil pathway should be reported
394 as E_{SOIL} .

395 Specific resistance terms for the soil deposition pathway and the lower canopy pathway have not been requested
396 because the resistance frameworks for these pathways vary considerably across models and therefore specific
397 resistance terms are not easily comparable. For example, Wesely (1989) used a single term for the soil resistance
398 (Fig. 1) while other models may use two or three resistances related to dry deposition to soil only and added in series
399 (Fig. 2).

400 In addition to the effective conductances, another set of diagnostic fields is calculated during post processing: the
401 time-aggregated fractional mass (or charge equivalent) *flux* transferred to the surface via each of the four deposition
402 pathways (hereinafter, *effective flux*). The effective flux is calculated on an hourly basis prior to conversion to
403 AQMEII4 time-aggregated gridded and station data using ENFORM, and is the product of the hourly effective
404 conductances, dry deposition mass fluxes, and inverses of the deposition velocity. Effective *conductances* provide
405 an estimate of the importance of each pathway towards the deposition velocity. However, since the flux depends
406 on the deposition velocity and the near-surface air concentration, which both vary on hourly timescales, estimating
407 the aggregate importance of each deposition pathway towards the flux requires calculating the effective flux before
408 time-aggregation.

409 Figure 3 provides an example of the different yet complementary information resulting from effective conductances
410 and effective fluxes, showing hourly SO_2 concentrations, effective conductances, and effective fluxes for a boreal
411 forest impacted by a large industrial SO_2 stack sources, and hourly NO_2 concentrations, effective conductances, and
412 effective fluxes for a location to the north-east of New York City. In both cases, high concentrations of the pollutant
413 gas (Fig. 3a,d) occur at night, while the deposition velocity, due to the stomatal pathway (Fig. 3b,e), maximizes during
414 the day. As a result of the low daytime concentrations, the effective fluxes for SO_2 (Fig. 3c) show a relatively minor
415 contribution of the stomatal pathway to the deposited mass despite the major contribution of the stomatal pathway
416 to the daytime deposition velocity. As the result of high night and morning concentrations, the effective fluxes for
417 NO_2 (Fig. 3f) show separate day and night peaks of about equal magnitude, with the stomatal pathway dominating
418 daytime values, and roughly equivalent contributions from stomatal and soil pathways at night.



419

420 **Figure 3. Two examples of diurnal variations in concentrations (a, d), effective conductances (b, e), and effective**
421 **fluxes (c, f) for SO₂ (top row) and NO₂ (bottom row).**

422 We also consider that dry deposition strongly depends on LULC type, and different models use unique LULC
423 databases. We thus request LULC-specific variables along with the fractional areal coverage for each LULC type,
424 which allows quantifying not only the impacts of different LULC specific processes and parameters on dry deposition,
425 but also the impacts of different LULC databases. ‘Generic’ AQMEI4 LULC types were devised due to the use of a
426 wide variety of LULC databases across air quality models, both in terms of the source of the data and the number of
427 LULC types employed. The AQMEI4 LULC types listed in Table 2 are broad LULC types into which the model-specific
428 LULC types could be aggregated, to allow intercomparison between models. Study participants aggregated their
429 LULC-model-specific diagnostic outputs to the set of common AQMEI4 LULC types using the fractional
430 representation of each native LULC type contributing to the AQMEI4 type within each grid cell. Generic AQMEI4
431 LULC types were constructed after analysis of the LULC schemes in the participating models. A suggested mapping
432 between model and AQMEI4 LULC types was provided to participants, along with the instruction that the mapping
433 actually employed should be reported. The grid cell fractions of both the native model LULC types, as well as the
434 resulting fractions of AQMEI4 LULC types, were reported by participants. Note that there is a large variety in number
435 and therefore types of LULC across models, and thus each of the generic types represents a rather broad range
436 of LULCs.

437 For AQMEI4, the terms listed in Table 4 were reported for SO₂, NO₂, NO, HNO₃, NH₃, PAN, HNO₄, N₂O₅, organic
438 nitrates, O₃, H₂O₂ and HCHO, both as a function of the 16 generic AQMEI4 LULC types (Table 3) as well as for the net
439 grid-scale calculation for each grid cell and/or receptor. Models employing bidirectional flux algorithms for the dry
440 deposition of atmospheric NH₃ reported a different set of terms, given in Section 4.2.



441

Generic LULC Categories for Remapping
Water
Developed / Urban
Barren
Evergreen needleleaf forest
Deciduous needleleaf forest
Evergreen broadleaf forest
Deciduous broadleaf forest
Mixed forest
Shrubland
Herbaceous
Planted/Cultivated
Grassland
Savanna
Wetlands
Tundra
Snow and Ice

442

443 **Table 3 Generic land use / land cover types for AQMEI4**

444 Table 4 summarizes the diagnostic variables related to gaseous dry deposition reported by all participants, the
445 variable names as described in the AQMEI4 TSDs, and a description of each variable. Equations (2) through (6) and
446 the related text describe the terms specifically for the resistance framework of Wesely (1989); additional examples
447 for participating models' resistance frameworks are provided in the Appendix tables and figures.

448 The presence of surface wetness or snow is incorporated into the effective conductance, effective flux, and
449 component resistances. In other words, separate component resistances or effective conductances and fluxes for
450 snow-covered or wet surfaces were not reported. In order to compare the impacts of the different models'
451 predictions regarding snow cover or wetness, additional diagnostic variables were requested to describe surface
452 state (e.g. fractional snow cover and either the values of binary wet/dry conditions or fractions in surface wetness).

Name	AQMEI4 Name	Formula
V_d	VD	Deposition velocity
r_a	RES-AERO	Aerodynamic resistance
r_c	RES-SURF	Bulk surface resistance



r_s	RES-STOM	Stomatal resistance
r_m	RES-MESO	Mesophyll resistance
r_c	RES-CUT	Cuticle resistance
E_{STOM}	ECOND-ST	Effective conductance associated with deposition to plant stomata
E_{CUT}	ECOND-CUT	Effective conductance associated with deposition to leaf cuticles
E_{SOIL}	ECOND-SOIL	Effective conductance associated with deposition to soil and un-vegetated surfaces
E_{LCAN}	ECOND-LCAN	Effective conductance associated with deposition to the lower canopy
$r_{b, stom}$	RES-QLST	Quasi-laminar sublayer resistance associated with stomatal pathway*
$r_{b, cut}$	RES-QLCT	Quasi-laminar sublayer resistance associated with cuticular pathway*
$r_{b, soil}$	RES-QLSL	Quasi-laminar sublayer resistance associated with soil pathway*
$r_{b, lcan}$	RES-QLLC	Quasi-laminar sublayer resistance associated with lower canopy pathway*
r_{dc}	RES-CONV	Resistance associated with within-canopy buoyant convection
Post Processing Fields: Effective Conductances x Net flux / Deposition Velocity		
DFLX-LCAN		Fraction of flux via lower canopy pathway
DFLX-ST		Fraction of flux via stomatal pathway
DFLX-CUT		Fraction of flux via cuticle pathway
DFLX-SOIL		Fraction of flux via soil pathway

453 * = r_b if this is pathway-independent for the resistance framework

454 **Table 4. AQMEI14 reported dry deposition diagnostic variables for gas phase species.**

455 Gridded dry deposition diagnostic variables were archived as hourly values for the native LULC types, and then
 456 converted to the generic AQMEI14 LULC types during post-processing. The ENFORM Fortran code provided to all
 457 participants was used to convert gridded fields from the hourly values to temporal aggregations of the hourly values.
 458 Hourly diagnostics were converted to “monthly median diurnal” values using ENFORM by taking the medians of all
 459 values for a given UTC hour in a given month, thus reducing 8,760 hourly values for each year to 288 values (24 hours
 460 x 12 months). The use of monthly median diurnal values is motivated by the need to reduce the amount of data to
 461 be transferred and analyzed on a single server (despite this aggregation, each year of gridded model output requires
 462 up to 200 Gb of storage), while preserving the key aspects of diurnal and seasonal variations.

463 The use of a median rather than an arithmetic mean for AQMEI14 diagnostic time aggregation resulted from
 464 consideration of the manner in which different dry deposition algorithms deal with pathways that effectively shut
 465 down under certain conditions. For example, some algorithms employ an upper-limit resistance to represent
 466 conditions under which the pathway transmits little mass to the surface (e.g. nighttime stomatal resistances may be
 467 set to very large values). Others simply use code branching to prevent a pathway from contributing to r_c (e.g. the
 468 entire stomatal pathway is removed from r_c at night). Others employ different resistance frameworks for different
 469 conditions (e.g. to account for snow-covered surfaces). However, the AQMEI14 protocol requires participants to



470 submit “missing values” as a specific code (-9) in order to allow filtering of valid from invalid data during time
471 aggregation. An algorithm removing a pathway may thus have a different number of valid values from an algorithm
472 employing a large resistance. Similarly, a seasonal transition where the resistance network changes depending on
473 whether a surface is snow-covered becomes difficult to interpret in an time-average, whereas time-median valid
474 values allow for a more meaningful comparison.

475 For example, if only 20% of the resistances at 14:00 LT in a given month and grid cell are snow covered, then the
476 monthly median for 14:00 LT would represent values typical of snow-free conditions, both for models representing
477 resistances under snow-covered conditions as missing, and models representing them as large values. Thus, the
478 monthly median comparison represents the most common conditions encountered during the month for both
479 models. On the other hand, while the monthly average resistance for 14:00 LT represents snow-free conditions for
480 the model that treats snow-covered hours as missing, the monthly average for the model that represents snow-
481 covered conditions as a large value is not meaningful and complicates inter-model comparison.

482 Monthly median diurnal values capture both seasonal and diurnal variations in the archived fields and allow
483 comparisons between algorithms shutting off a pathway by removing the pathway and algorithms shutting off a
484 pathway with high resistance values. Note that the same data completeness criterion used for comparing simulated
485 and observed ambient concentrations was employed here for the construction of the median values. Specifically,
486 more than 75% of the values within a month were required for a median to be constructed.

487 **4. More Example Calculations of AQMEI4 Dry Deposition Variables.**

488 **4.1 Variations to the Wesely (1989) Resistance Framework**

489 For the sake of clarity, we provide examples of how specific dry deposition schemes can be reduced to the common
490 set of variables described above. The generic schemes presented in Fig. 2a,b along with the Nemitz et al. (2001)
491 bidirectional scheme for NH₃ have been selected as examples here, while Appendix B provides additional examples
492 for specific schemes implemented in participating models. The AQMEI4 protocol and these specific examples
493 provide a standard form of representing key aspects of dry deposition schemes, which may be adopted by similar
494 activities or initiatives in the future. Note that some of these example algorithms do not have a separate resistance
495 for lower canopy buoyant convection or a deposition pathway to the lower canopy and exposed surfaces, hence the
496 associated effective conductance (ECOND-LCAN) and resistance (RES-CONV and RES-QLLC) terms are not reported.

Na me	AQMEI4 Name	Formula
r_a	RES-AERO	$RES-AERO = r_a$
r_c	RES-SURF	$RES-SURF = \left((r_{leaf1} + ((r_{stom1} + r_m)^{-1} + (r_{cut1})^{-1})^{-1})^{-1} + (r_{soil1} + r_{soil2} + r_{soil3})^{-1} \right)^{-1}$
r_s	RES-STOM	$RES-STOM = r_{stom1}$



r_m	RES-MESO	$RES-MESO = r_m$
r_c	RES-CUT	$RES-CUT = r_{cut1}$
E_{STO} M	ECOND-ST	$ECOND-ST = \left(\frac{(r_{stom1} + r_m)^{-1}}{(r_{stom1} + r_m)^{-1} + (r_{cut1})^{-1}} \right) \left(\frac{(r_{leaf1} + ((r_{stom1} + r_m)^{-1} + (r_{cut1})^{-1})^{-1})^{-1}}{(r_{leaf1} + ((r_{stom1} + r_m)^{-1} + (r_{cut1})^{-1})^{-1})^{-1} + (r_{soil1} + r_{soil2} + r_{soil3})^{-1}} \right) V_d$
E_{CUT}	ECOND-CUT	$ECOND-CUT = \left(\frac{(r_{cut1})^{-1}}{(r_{stom1} + r_m)^{-1} + (r_{cut1})^{-1}} \right) \left(\frac{(r_{leaf1} + ((r_{stom1} + r_m)^{-1} + (r_{cut1})^{-1})^{-1})^{-1}}{(r_{leaf1} + ((r_{stom1} + r_m)^{-1} + (r_{cut1})^{-1})^{-1})^{-1} + (r_{soil1} + r_{soil2} + r_{soil3})^{-1}} \right) V_d$
E_{SOIL}	ECOND-SOIL	$ECOND-SOIL = \left(\frac{(r_{soil1} + r_{soil2} + r_{soil3})^{-1}}{(r_{leaf1} + ((r_{stom1} + r_m)^{-1} + (r_{cut1})^{-1})^{-1})^{-1} + (r_{soil1} + r_{soil2} + r_{soil3})^{-1}} \right) V_d$
E_{LCA} N	ECOND-LCAN	$ECOND-LCAN = -9$
$r_{b,sto}$ m	RES-QLST	$RES-QLST = r_{leaf1}$
$r_{b,cut}$	RES-QLCT	$RES-QLCT = r_{leaf1}$
$r_{b,soi}$ l	RES-QLSL	$RES-QLCL = r_{soil2}$
$r_{b,lca}$ n	RES-QLLC	$RES-QLLC = -9$
r_{dc}	RES-CONV	$RES-CONV = -9$

497 Table 5. AQMEI4 dry deposition diagnostic variables for gas phase species corresponding to the resistance
 498 framework of Fig. 2a.

499



500

Name	AQMEI4 Name	Formula
r_a	RES-AERO	$RES-AERO = r_a$
r_c	RES-SURF	$RES-SURF = ((r_s + r_m)^{-1} + (r_{lu})^{-1} + (r_{soil1} + r_{soil2})^{-1})^{-1}$
r_s	RES-STOM	$RES-STOM = r_s$
r_m	RES-MESO	$RES-MESO = r_m$
r_c	RES-CUT	$RES-CUT = r_{lu}$
E_{STOM}	ECOND-ST	$ECOND-ST = \left(\frac{(r_s + r_m)^{-1}}{(r_s + r_m)^{-1} + (r_{lu})^{-1} + (r_{soil1} + r_{soil2})^{-1}} \right) V_d$
E_{CUT}	ECOND-CUT	$ECOND-CUT = \left(\frac{(r_{lu})^{-1}}{(r_s + r_m)^{-1} + (r_{lu})^{-1} + (r_{soil1} + r_{soil2})^{-1}} \right) V_d$
E_{SOIL}	ECOND-SOIL	$ECOND-SOIL = \left(\frac{(r_{soil1} + r_{soil2})^{-1}}{(r_s + r_m)^{-1} + (r_{lu})^{-1} + (r_{soil1} + r_{soil2})^{-1}} \right) V_d$
E_{LCAN}	ECOND-LCAN	$ECOND-LCAN = -9$
$r_{b, stom}$	RES-QLST	$RES-QLST = r_b$
$r_{b, cut}$	RES-QLCT	$RES-QLCT = r_b$
$r_{b, soil}$	RES-QLSL	$RES-QLSL = r_b$
$r_{b, lcan}$	RES-QLLC	$RES-QLLC = -9$
r_{dc}	RES-CONV	$RES-CONV = -9$

501

502 **Table 6. AQMEI4 dry deposition diagnostic variables for gas phase species corresponding to the resistance**
 503 **framework of Fig. 2b.**

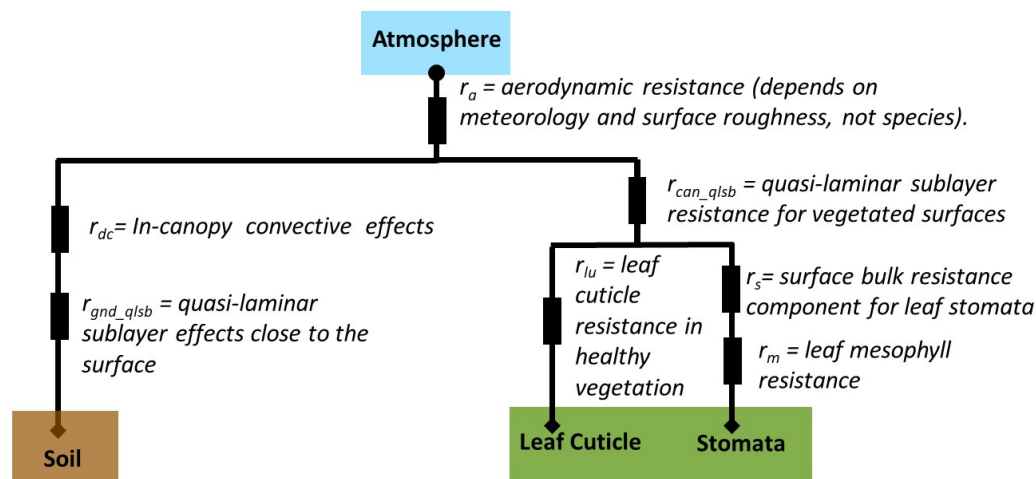
504 **4.2 Bidirectional fluxes of ammonia – a special case**

505 Some models make use of the concepts of bidirectional fluxes when describing ammonia gas transfer from and to
 506 surfaces. In the bidirectional flux paradigm, the difference between the ambient gas concentrations and near-
 507 surface (compensation point) concentration is used to determine the direction of the flux: if the ambient air
 508 concentration is greater than the compensation point concentration, the flux is downward (i.e. deposition occurs)
 509 while in the reverse case the flux is upward (i.e. the emission of ammonia previously stored in the surfaces takes
 510 place). The algorithms used in the subset of models employing ammonia bidirectional fluxes were examined, in
 511 order to determine common terms that could be used for points of comparison across the algorithms. As an
 512 example, we present below (Figure 4 and Table 7) the bidirectional flux model of Nemitz et al. (2001), used within
 513 CMAQ to represent bidirectional ammonia gas fluxes. In addition, we also include a comparison of two ammonia
 514 bidirectional flux calculations in Appendix C.

515 The bidirectional flux algorithms were analyzed as a separate case, with the result that a revised and smaller number
 516 of variables were reported for the specific case of ammonia bidirectional fluxes than for other gases, focusing on the
 517 compensation point concentrations as diagnostics for the cross-comparison of these algorithms. The reported



518 variables in this case are ammonia's aerodynamic resistance, its net surface resistance, and three compensation
 519 point concentrations, for stomata, ground and net compensation points, respectively. These specific parameters for
 520 ammonia bidirectional fluxes appear in Table 7, and a detailed comparison of two representative bidirectional
 521 ammonia algorithms is presented in Appendix C.



522

523 **Figure 4. Nemitz bidirectional flux model for NH_3 .**

524 In this example, note that the branch containing the r_{dc} term has been designated as the lower canopy pathway, due
 525 to the presence of the canopy buoyant convection term r_{dc} (i.e., closest analogy to Wesely's setup is to have the
 526 pathway involving deposition to "soil" pathway is designated as a "lower canopy" pathway).

527 Table 7. Variables for bidirectional fluxes of ammonia.

Name as described here	AQMEI14 Variable Name	Details
r_{sum}	RES-SUM-NH3	Net bidirectional flux ammonia resistance
r_a	RES-AERO-NH3	Net Aerodynamic resistance used for ammonia bidirectional fluxes
c_a	CONC-NH3-AIR	Air concentration of ammonia used for bidirectional flux calculations
c_c	COMP-NH3-NET	Net Ammonia Overall Compensation point concentration
c_g	COMP-NH3-GND	Net Ammonia Compensation point concentration with respect to ground
c_s	COMP-NH3-STO	Net Ammonia Compensation point concentration with respect to stomata

528

529

530



531

532 **Conclusions**

533 The fourth phase of the Air Quality Model International Initiative has been introduced. The focus of this phase is on
534 wet and especially dry deposition. The necessity of tackling this subject in a diagnostic way prompted us to divide
535 the initiative in two activities, one dedicated to the evaluation of the process as described by 4-dimensional air
536 quality regional-scale models, the second dealing specifically with evaluating ozone dry deposition calculated by
537 “single-point model” versions of the dry deposition modules used in the regional-scale models with a collection of
538 ozone flux measurements. Here, the organization of Activity 1 has been formally introduced, whereas Activity 2 is
539 presented in a separate companion technical note. In addition to presenting the standard and common input data
540 and the way in which standard output is expected, we also presented the way in which the very diverse
541 representations of dry deposition in participating models have been reduced to a common representation that will
542 facilitate model inter-comparison. The essence of the adopted methodology is the transformation of individual
543 resistances into effective conductances and effective fluxes, which represent the importance of deposition pathways
544 held in common across the models to the total deposition velocity and flux. Resistances held in common across
545 different modelling frameworks were also reported, to allow comparisons at the sub-pathway level, where possible.
546 Thus, regardless of the level of sophistication of the resistance framework, one can meaningfully inter-compare the
547 results produced by different models.

548

549 **Data availability.**

550 No data was generated for this technical note

551

552 **Author contributions.**

553 SG, PM, OEC, and CH led the writing of this technical note. SG, PM, OEC, CH, RB, RB, JB, JD, JF, CDH, IK, DS, and SS
554 conceptualized and implemented the AQMEII4 modeling and analysis framework. JOB, TB, AH, RK, AL, JLPC, JP< YHR,
555 RSJ, MG, and RW provided documentation of dry deposition schemes used in their models.

556

557 **Competing interests.**

558 The authors declare no conflict of interest

559

560 **Acknowledgments**



561 We gratefully acknowledge the contribution of various groups to the fourth AQMEII activity. The following groups
562 contributed the data sets used in the grid modeling aspects of this study: U.S. EPA and Environment and Climate
563 Change Canada (North American emissions processing); TNO (European emissions processing); ECMWF and
564 Copernicus Atmosphere Monitoring Service (Chemical boundary conditions); ECCAD (archiving and distribution of
565 the GEIA lightning emissions data based on Price et al. (1997)); Finnish Meteorological Institute (European wildfire
566 emissions). Ambient North American concentration measurements were extracted from Environment Canada's
567 National Atmospheric Chemistry Database (NAtChem) PM database and provided by several U.S. and Canadian
568 agencies (AQS, CAPMoN, CASTNet, IMPROVE, NAPS, SEARCH and CSN networks); North American precipitation-
569 chemistry measurements were extracted from NAtChem's precipitation-chemistry data base and were provided by
570 several U.S. and Canadian agencies (CAPMoN, NADP, NBPMN, NSPSN, and REPQ networks); the WMO World Ozone
571 and Ultraviolet Data Centre (WOUDC) and its data-contributing agencies provided North American and European
572 ozonesonde profiles; for European air quality data the following data centers were used: EMEP European
573 Environment Agency/European Topic Center on Air and Climate Change/AirBase provided European air- and
574 precipitation-chemistry data. Data from meteorological station monitoring networks were obtained from NOAA and
575 Environment and Climate Change Canada (for the US and Canadian meteorological network data) and the National
576 Center for Atmospheric Research (NCAR) Data Support Section. The Joint Research Center Ispra/Institute for
577 Environment and Sustainability provided its ENSEMBLE system for model output harmonization and analyses and
578 evaluation.

579 **Disclaimer**

580 The views expressed in this paper are those of the authors and do not necessarily represent the view or policies of
581 the U.S. Environmental Protection Agency. This material is based upon work supported, in part, by the National
582 Center for Atmospheric Research, which is a major facility sponsored by the National Science Foundation under
583 Cooperative Agreement No. 1852977.

584 **References**

- 585 Anav, A., Proietti, C., Menut, L., Carnicelli, S., De Marco, A., & Paoletti, E. (2018). Sensitivity of stomatal conductance
586 to soil moisture: implications for tropospheric ozone. *Atmospheric Chemistry and Physics*, 18, 5747-5763.
587 <https://doi.org/10.5194/acp-18-5747-2018>
- 588 Andersson, C., and M. Engardt (2010), European ozone in a future climate: Importance of changes in dry deposition
589 and isoprene emissions, *J. Geophys. Res.*, 115, D02303, doi:10.1029/2008JD011690.
- 590 Bash, J.O., Walker, J.T., Katul, G.G., Jones, M.R., Nemitz, E., Robarge, W.P., Estimation of in-canopy ammonia sources
591 and sinks in a fertilized Zea mays field, *Environ. Sci. Technol.*, 44, 1683-1689, 2010
- 592 Bash, J.O., Cooter, E.J., Dennis, R.W., Walker, J.T., Pleim, J.W., Evaluation of a regional air-quality model with bi-
593 directional NH₃ exchange coupled to an agro-ecosystem model, *Biogeosci.*, 10, 1635-1645
- 594 Baublitz, C. B., A. M. Fiore, O. E. Clifton, J. Mao, J. Li, G. Correa, D. Westervelt, L. W. Horowitz, F. Paulot, R. Commane,
595 & A. P. Williams (2020). Sensitivity of tropospheric ozone over the Southeast USA to dry deposition. *Geophysical*
596 *Research Letters*. <https://doi.org/10.1029/2020GL087158>



- 597 Beddows, A. V., Kitwiroon, N., Williams, M. L., & Beevers, S. D. (2017). Emulation and sensitivity analysis of the
598 community multiscale air quality model for a UK Ozone pollution episode. *Environmental Science & Technology*,
599 *51*(11), 6229-6236.
- 600 Blakeslee, R.J., Mach, D.M., Bateman, M.G., Bailey, J.C. Seasonal variations in the lightning diurnal cycle and
601 implications for the global electric circuit, *Atmospheric Research*, 228-243,
602 <https://doi.org/10.1016/j.atmosres.2012.09.023>, 2014.
- 603 Borrell, P., and P. M. Borrell (eds), 2000. Transport and Chemical Transformation of Pollutants in the Troposphere,
604 An Overview of the Work of EUROTRAC, <https://doi.org/10.1007/978-3-642-59718-3>, Springer, Berlin, 474 pp.
- 605 Briggs, Gary A., 1971: Some Recent Analyses of Plume Rise Observation, pp. 1029-1032 in Proceedings of the Second
606 International Clean Air Congress, edited by H. M. Englun and W. T. Beery. Academic Press, New York.
- 607 Briggs, Gary A., 1972: Discussion on Chimney Plumes in Neutral and Stable Surroundings, *Atmos. Environ.* 6, 507-
608 510.
- 609 Campbell, P. C., Bash, J. O., & Spero, T. L. (2019). Updates to the Noah Land Surface Model in WRF-CMAQ to improve
610 simulated meteorology, air quality, and deposition. *Journal of Advances in Modeling Earth Systems*, *11*, 231-
611 256. <https://doi.org/10.1029/2018MS001422>
- 612 Chang, J. S., Brost, R. A., Isaksen, I. S. A., Madronich, S., Middleton, P., Stockwell, W. R., and Walcek, C. J., 1987. A
613 three-dimensional Eulerian acid deposition model: Physical concepts and formulation *J. Geo. Res.* 92, 14,681-
614 14,700
- 615 Clifton, O. E., Fiore, A. M., Munger, J. W., Malyshev, S., Horowitz, L. W., Shevliakova, E., et al.: Interannual variability
616 in ozone removal by a temperate deciduous forest, *Geophys. Res. Lett.*, *44*, 542-
617 552, <https://doi.org/10.1002/2016GL070923>, 2017.
- 618 Clifton, O. E., Fiore, A. M., Massman, W. J., Baublitz, C. B., Coyle, M., Emberson, L., et al.: Dry deposition of ozone
619 over land: processes, measurement, and modeling, *Rev. Geophys.*, *58*, <https://doi.org/10.1029/2019RG000670>,
620 2020.
- 621 Clifton, O. E., Paulot, F., Fiore, A. M., Horowitz, L. W., Correa, G., Fares, S., Goded, I., Goldstein, A. H., Gruening, C.,
622 Hogg, A. J., Loubet, B., Mammarella, I., Munger, J. W., Neil, L., Stella, P., Uddling, J., Vesala, T., & Weng, E.
623 (2020b). Influence of dynamic ozone dry deposition on ozone pollution. *Journal of Geophysical Research:*
624 *Atmospheres*. <https://doi.org/10.1029/2020JD032398>
- 625 Dennis, R., Fox, T., Fuentes, M. *et al.* A framework for evaluating regional-scale numerical photochemical modeling
626 systems. *Environ Fluid Mech* *10*, 471-489 (2010). <https://doi.org/10.1007/s10652-009-9163-2>
- 627 Dizengremel P., D. Le Thiec, M. Bagard, Y. Jolivet, Ozone risk assessment for plants: central role of metabolism-
628 dependent changes in reducing power, *Environ. Pollut.*, *156* (2008), pp. 11-15
- 629 Emberson, L. D., Nitwiroon, N., Beevers, S., Büker, P., & Cinderby, S. (2013). Scorched Earth: how will changes in the
630 strength of the vegetation sink to ozone deposition affect human health and ecosystems? *Atmospheric*
631 *Chemistry and Physics*, *13*, 6741-6755. <https://doi.org/10.5194/acp-13-6741-2013>
- 632 Emberson L. D, Håkan Pleijel, Elizabeth A. Ainsworth, Maurits van den Berg, Wei Ren, Stephanie Osborne, Gina Mills,
633 Divya Pandey, Frank Dentener, Patrick Büker, Frank Ewert, Renate Koeble, Rita Van Dingenen, Ozone effects on
634 crops and consideration in crop models, *European Journal of Agronomy*, *100*, 2018, 19-34
- 635 Emerson, E.W., A.L. Hodshire, H.M. DeBolt, K.R. Bilsback, J.R. Pierce, G.R. McMeeking, D.K. Farmer, Revisiting particle
636 dry deposition and its role in radiative effect estimates, Proceedings of the National Academy of Sciences, 2020,
637 *117* (42) 26076-26082; DOI: 10.1073/pnas.2014761117



- 638 Erisman, J.W., Evaluation of a surface resistance parameterization for sulphur dioxide, *Atmos. Environ.*, 28(16), 2583-
639 2594, 1994
- 640 Galmarini S., ST Rao, D.G. Steyn, Preface, *Atmos. Environ.* 53, 2012
- 641 Galmarini S., C. Hogrefe, D. Brunner, P. Makar, A. Baklanov, Preface, *Atmospheric Environment* 115, 2015
- 642 Galmarini S., Brigitte Koffi, Efisio Solazzo, Terry Keating, Christian Hogrefe, Michael Schulz, Anna Benedictow, Jan
643 Jurgen Griesfeller, Greet Janssens-Maenhout, Greg Carmichael, Joshua Fu, and Frank Dentener, *Atmos. Chem.*
644 *Phys.*, 17, 1543–1555, 2017
- 645 Hardacre, C. and Wild, O. and Emberson, L. An evaluation of ozone dry deposition in global scale chemistry climate
646 models, *Atmospheric Chemistry and Physics*, 15, 2015, 11, 6419—6436
- 647 Hogrefe, C., Liu, P., Pouliot, G., Mathur, R., Roselle, S., Flemming, J., Lin, M., and Park, R. J.: Impacts of different
648 characterizations of large-scale background on simulated regional-scale ozone over the continental United
649 States, *Atmos. Chem. Phys.*, 18, 3839–3864, <https://doi.org/10.5194/acp-18-3839-2018>, 2018.
- 650 Hogrefe C. et al. (2020) Continental-Scale Analysis of Atmospheric Deposition Over North America and Europe Using
651 the AQMEII Database. In: Mensink C., Gong W., Hakami A. (eds) *Air Pollution Modeling and its Application XXVI*.
652 ITM 2018. Springer Proceedings in Complexity. Springer, Cham. https://doi.org/10.1007/978-3-030-22055-6_48
- 653 Hong, C., Mueller, N.D., Burney, J.A., Zhang, Y., AghaKouchak, A., Moore, F.C., Qin, Y., Tong, D. and Davis, S.J., 2020.
654 Impacts of ozone and climate change on yields of perennial crops in California. *Nature Food*, 1(3), pp.166-172.
- 655 Huang, L., McDonald-Buller, E. C., McGaughey, G., Kimura, Y., & Allen, D. T. (2016). The impact of drought on ozone
656 dry deposition over eastern Texas. *Atmospheric Environment*, 127, 176-186.
657 <https://doi.org/10.1016/j.atmosenv.2015.12.022>
- 658 Inness, A., Ades, M., Agustí-Panareda, A., Barré, J., Benedictow, A., Blechschmidt, A.-M., Dominguez, J. J., Engelen,
659 R., Eskes, H., Flemming, J., Huijnen, V., Jones, L., Kipling, Z., Massart, S., Parrington, M., Peuch, V.-H., Razinger,
660 M., Remy, S., Schulz, M., and Suttie, M.: The CAMS reanalysis of atmospheric composition, *Atmos. Chem. Phys.*,
661 19, 3515-3556, <https://doi.org/10.5194/acp-19-3515-2019>, 2019.
- 662 Irving, P.M., & Smith, E. (1991). *Acid deposition: State of science and technology Summary report of the US National*
663 *Acid Precipitation Assessment Program*, US Govt. Printing Office, ISBN 0-16-035925-2, 274pp., United States.
- 664 Jarvis, P. G.: The interpretation of the variations in leaf water potential and stomatal conductance found in canopies
665 in the field, *Phil. Trans. R. Soc. Lond. B.*, 273, 593–610, 1976.
- 666 Knote, C., Hodzic, A., and Jimenez, J. L., The effect of dry and wet deposition of condensable vapors on secondary
667 organic aerosols concentrations over the continental US, *Atmos. Chem. Phys.*, 15, 1-18,
668 <https://doi.org/10.5194/acp-15-1-2015>, 2015.
- 669 Kuenen, J., A. Visschedijk, H.A.C. Denier van der Gon. TNO_MACC-III inventory and its application for FAIRMODE
670 SoAp, Fairmode technical meeting, Aveiro, Portugal, June 2015,
671 [https://aqm.jrc.ec.europa.eu/fairmode/document/event/presentation/20150624-](https://aqm.jrc.ec.europa.eu/fairmode/document/event/presentation/20150624-Aveiro/WG3/WG3%20Kuenen.pdf)
672 [Aveiro/WG3/WG3%20Kuenen.pdf](https://aqm.jrc.ec.europa.eu/fairmode/document/event/presentation/20150624-Aveiro/WG3/WG3%20Kuenen.pdf)
- 673 Lin, M., Horowitz, L. W., Xie, Y., Paulot, F., Malyshev, S., Shevliakova, E., ... & Pilegaard, K. (2020). Vegetation
674 feedbacks during drought exacerbate ozone air pollution extremes in Europe. *Nature Climate Change*, 10(5),
675 444-451
- 676 Lombardozzi, D., Levis, S., Bonan, G., Hess, P. G., & Sparks, J. P. (2015). The Influence of Chronic Ozone Exposure on
677 Global Carbon and Water Cycles. *Journal of Climate*, 28(1), 292–305. [https://doi.org/10.1175/JCLI-D-14-](https://doi.org/10.1175/JCLI-D-14-00223.1)
678 [00223.1](https://doi.org/10.1175/JCLI-D-14-00223.1)



- 679 Makar, P.A., Akingunola, A., Aherne, J., Cole, A.S., Aklilu, Y.-A., Zhang, J., Wong, I., Hayden, K., Li, S.-M., Kirk, J., Scott,
680 K., Moran, M.D., Robichaud, A., Cathcart, H., Baratzedah, P., Pabla, B., Cheung, P., Zheng, Q., Jeffries, D.S.,
681 Estimates of exceedances of critical loads for acidifying deposition in Alberta and Saskatchewan, *Atmos. Chem.*
682 *Phys.*, 18, 9897-9927, 2018.
- 683 Matichuk, R., Tonnesen, G., Luecken, D., Gilliam, R., Napelenok, S. L., Baker, K. R., et al. (2017). Evaluation of the
684 Community Multiscale Air Quality Model for simulating winter ozone formation in the Uinta Basin. *Journal of*
685 *Geophysical Research: Atmospheres*, 122(24), 13545-13572. <https://doi.org/10.1002/2017JD027057>
- 686 Massad, R-S., Nemitz, E., Sutton, M.A., Review and parameterization of bi-directional ammonia exchange between
687 vegetation and the atmosphere, *Atmos. Chem. Phys.*, 10, 10359-10386, 2010
- 688 McGrath, J. M., Betzelberger A. M., Wang, S., Shook, E., Zhu, X. G., Long, S. P., and Ainsworth, E. A.: An analysis of
689 ozone damage to historical maize and soybean yields in the United States, *Proc. Natl. Acad. Sci.*, 112, 14390–5,
690 2015.
- 691 Nemitz, E., Sutton, M.A., Schjoerring, J.K., Husted, S., Wyers, G.P., Resistance modelling of ammonia exchange over
692 oilseed rape, *Agriculture and Forest Meteorology*, 105, 405-425, 2000
- 693 Nemitz, E., Milford, C., Sutton, M.A., A two-layer canopy compensation point model for describing bi-directional
694 biosphere-atmosphere exchange of ammonia, *Q. J. Roy. Meteor. Soc.*, 127, 815-833, 2001
- 695 Oliver, R. J., Mercado, L. M., Sitch, S., Simpson, D. M., Medlyn, B. E., Lin, Y., and Folberth, G. A.: Large but decreasing
696 effect of ozone on the European carbon sink, *Biogeosciences*, 4245-4269, 2018.
- 697 Ott, L. E., K. E. Pickering, G. L. Stenchikov, D. J. Allen, A. J. DeCaria, B. Ridley, R.-F. Lin, S. Lang, and W.-K. Tao (2010),
698 Production of lightning NO_x and its vertical distribution calculated from three-dimensional cloud-scale chemical
699 transport model simulations, *J. Geophys. Res.*, 115, D04301, doi:10.1029/2009JD011880
- 700 Paulot, F., Malyshev, S., Nguyen, T., Crouse, J. D., Shevliakova, E., & Horowitz, L. W. (2018). Representing sub-grid
701 scale variations in nitrogen deposition associated with land use in a global Earth system model: implications for
702 present and future nitrogen deposition fluxes over North America. *Atmospheric Chemistry and Physics*, 18(24),
703 17963-17978.
- 704 Pleim, J.E., Bash, J.O., Walker, J.T., Cooter, E.J., Development and evaluation of an ammonia bidirectional flux
705 parameterization for air quality models, *J. Geophys. Res. Atm.*, 118, 3794-3806, 2013.
- 706 Pleim, J. E., Ran, L., Appel, W., Shephard, M. W., & Cady-Pereira, K. (2019). New bidirectional ammonia flux model
707 in an air quality model coupled with an agricultural model. *Journal of Advances in Modeling Earth Systems*, 11,
708 2934– 2957. <https://doi.org/10.1029/2019MS001728>
- 709 Price, C.G., J.E. Penner and M.J. Prather NO_x from lightning, Part I: Global distribution based on lightning physics
710 *Journal of Geophysical Research* 102 5229-5241 1997.
- 711 Rao, S.T., Galmarini, S., Puckett, K., 2011. *Air quality model evaluation international initiative (AQMEII)* . Bulletin of
712 the American Meteorological Society 92, 23-30. DOI:10.1175/2010BAMS3069.1
- 713 Robichaud, A., Cole, A., Moran, M., Lupu, A., Shaw, M., Roy, G., Beauchemin, M., Fortin, V., and Vet, R., Total
714 deposition maps evaluated from measurement-model fusion in North America (ADAGIO Project), In: Mensink
715 C., Gong W., Hakami A. (eds) *Air Pollution Modeling and its Application XXVI*. ITM 2018. Springer
716 Proceedings in Complexity. Springer, Cham. https://doi.org/10.1007/978-3-030-22055-6_40
- 717 Robichaud, A., Cole, A.S., Moran, M.D., Lupu, A., Beauchemin, M., and Fortin, V., On model-data fusion
718 approaches for wet deposition in North America, National Atmospheric Deposition Program Scientific
719 Symposium and Fall Meeting, October 28-30, 2020; <http://nadp.slh.wisc.edu/conf/2020/?slid=6>, last
720 accessed March 23, 2021.



- 721 Schiferl, L. D., and C. L. Heald. "Particulate Matter Air Pollution May Offset Ozone Damage to Global Crop
722 Production." *Atmos. Chem. Phys.* 18, no. 8 (April 27, 2018): 5953–66. [https://doi.org/10.5194/acp-18-5953-
723 2018](https://doi.org/10.5194/acp-18-5953-2018)
- 724 Schwede, D.B. and G.G. Lear, 2014 A novel hybrid approach for estimating total deposition in the United States.
725 *Atmospheric Environment*, 92, 207–220
- 726 Sharma, A., Ojha, N., Ansari, T. U., Sharma, S. K., Pozzer, A., & Gunthe, S. S. (2020). Effects of dry deposition on
727 surface ozone over South Asia inferred from a regional chemical transport model. *ACS Earth and Space
728 Chemistry*, 4(2), 321-327.
- 729 Sitch, S., Cox, P. M., Collins, W. J., & Huntingford, C. (2007). Indirect radiative forcing of climate change through
730 ozone effects on the land-carbon sink. *Nature*, 448(7155), 791–794. <https://doi.org/10.1038/nature06059>
- 731 Shuttleworth, W.J., Wallace, J.S., Evaporation from sparse crops – an energy combination theory, *Q. J. Roy. Meteor.
732 Soc.*, 111, 839-855, 1985
- 733 Silva, S. J., & Heald, C. L.: Investigating dry deposition of ozone to vegetation. *Journal of Geophysical Research:
734 Atmospheres*, 123, 559– 573. <https://doi.org/10.1002/2017JD027278>, 2018.
- 735 Soares, J., M. Sofiev, J. Hakkarainen, 2015. Uncertainties of wild-land fires emission in AQMEII phase 2 case study,
736 *Atmospheric Environment*, 115, 361-370, <https://doi.org/10.1016/j.atmosenv.2015.01.068>
- 737 Solazzo E., Angelo Riccio, Rita Van Dingenen, Luana Valentini, Stefano Galmarini, Evaluation and uncertainty
738 estimation of the impact of air quality modelling on crop yields and premature deaths using a multi-model
739 ensemble, *Science of The Total Environment*, 633, 2018, 1437-1452, 2018
- 740 Solazzo, E. and Hogrefe, C. and Colette, A. and Garcia-Vivanco, M. and Galmarini, S. , Advanced error diagnostics of
741 the CMAQ and Chimere modelling systems within the AQMEII3 model evaluation framework, *Atmospheric
742 Chemistry and Physics*, 17,2017,17,10435–10465
- 743 Solberg, S., Hov, Ø., Søvde, A., Isaksen, I. S. A., Coddevillee, P., De Backer, H., Forster, C., Orsolini, Y., & Uhse, K.
744 (2008). European surface ozone in the extreme summer 2003. *Journal of Geophysical Research*, 113(D07307).
745 <https://doi.org/10.1029/2007JD009098>
- 746 Val Martin, M., Heald, C.L., Arnold, S.R., Coupling dry deposition to vegetation phenology in the Community Earth
747 System Model: Implications for the simulation of surface O₃, *Geop. Res. Lett.*, 41, 2988-2996, 2014.
- 748 Vautard, R., Honore, C., Beekmann, M., & Rouil, L. (2005). Simulation of ozone during the August 2003 heat wave
749 and emission control scenarios. *Atmospheric Environment*, 39(16), 2957-2967.
- 750 Vivanco, M. G., Theobald, M. R., García-Gómez, H., Garrido, J. L., Prank, M., Aas, W., Adani, M., Alyuz, U., Andersson,
751 C., Bellasio, R., Bessagnet, B., Bianconi, R., Bieser, J., Brandt, J., Briganti, G., Cappelletti, A., Curci, G., Christensen,
752 J. H., Colette, A., Couvidat, F., Cuvelier, C., D'Isidoro, M., Flemming, J., Fraser, A., Geels, C., Hansen, K. M.,
753 Hogrefe, C., Im, U., Jorba, O., Kitwiroon, N., Manders, A., Mircea, M., Otero, N., Pay, M.-T., Pozzoli, L., Solazzo,
754 E., Tsyro, S., Unal, A., Wind, P., and Galmarini, S.: Modeled deposition of nitrogen and sulfur in Europe estimated
755 by 14 air quality model systems: evaluation, effects of changes in emissions and implications for habitat
756 protection, *Atmos. Chem. Phys.*, 18, 10199–10218, <https://doi.org/10.5194/acp-18-10199-2018>, 2018.
- 757 Wesely, M.L., Parameterization of surface resistances to gaseous dry deposition in regional-scale numerical models,
758 *Atmospheric Environment*, 23, 1293-1304, 1989.
- 759 Wu, Z., Schwede, D.B., Vet., R., Walker, J.T., Shaw, M., Staebler, R., and Zhang, L., Evaluation and intercomparison of
760 five North American dry deposition algorithms at a mixed forest site, *J. Adv. Mod. Earth Sys*, 10, 1571–1586.
761 <https://doi.org/10.1029/2017MS001231>, 2018.



- 762 Zhang, L., Moran, M.D., Makar, P.A., Brook, J.R., Gong, S., Modelling gaseous dry deposition in AURAMS: a unified
763 regional air-quality modelling system, *Atmos. Env.*, 36, 537-560, 2002.
- 764 Zhang, L., Brook, J.R., and Vet, R., A revised parameterization for gaseous dry deposition in air-quality models,
765 *Atmos. Chem. Phys.*, 3, 2067-2082, 2003.
- 766 Zhang, L., Wright, L. P., and Asman, W. A. H.: Bi-directional air-surface exchange of atmospheric ammonia: A review
767 of measurements and a development of a big-leaf model for applications in regional-scale air-quality models, *J.*
768 *Geophys. Res.*, 115, D20310, <https://doi.org/10.1029/2009JD013589>, 2010.
- 769
- 770
- 771



772 **Appendix A: Standard Output Requested From All Participating Models**

773 **Table A1 – AQMEII4 – Meteorology (grid)**

Variable	Description and Units
PRECIP	Sum of all surface precipitation, cm
PRESS	Surface pressure, hPa
MIXRAT	Water vapour mixing ratio @ 2 m, g kg ⁻¹
RH	Relative humidity @ 2 m, %
TD	Dew point temperature @ 2 m, K
TEMP	Air temperature @ 2 m, K
WS	Horizontal wind speed @ 10 m, m s ⁻¹
WD	Horizontal wind direction @ 10 m, deg
W	Vertical wind speed @ 10 m, m s ⁻¹
SWGU	Upward shortwave radiation at the ground, W m ⁻²
SWGDN	Downward Shortwave Radiation at the ground, W m ⁻²
SWTU	Upward shortwave radiation at atmosphere top, W m ⁻²
SWTD	Downward shortwave radiation at atmosphere top, W m ⁻²
PBL	Planetary boundary layer height, m
PAR	Photosynthetically active radiation at the ground, W m ⁻²
AOD470	Aerosol optical depth at 470 nm
AOD555	Aerosol optical depth at 555 nm
AOD675	Aerosol optical depth at 675 nm
H2O	Water vapor column, cm ³ cm ⁻²
USTAR	Friction velocity, m s ⁻¹
MOL	Monin-Obukhov length, m
RHO	Air density of lowest model layer
TEMP10	Air temperature at 10 m, K
TSOIL	Uppermost soil layer temperature, K
SNOWC	Fractional coverage of snow in grid cell, 0-1
WETCAN	Canopy wetness, 0.0 if dry and 1.0 if wet
SOILMOI	Uppermost soil layer moisture, m ³ m ⁻³
Z0	Surface roughness length, m
ALB	Albedo, fraction
Z	Terrain height above sea level, m
FWET	Wet surface, unitless fraction
LAI-T	Total leaf area index, m ² m ⁻²



774

775 **Table A2. AQMEI14 - Gas and Particle Concentrations and Emissions (grid)**

Variable	Description and Units
SO2	Concentration of SO ₂ at ground, µg m ⁻³
NO2	Concentration of NO ₂ at ground, µg m ⁻³
NO	Concentration of NO at ground, µg m ⁻³
NOx	Concentration of NO _x at ground, µg m ⁻³
NOy	Concentration of NO _y at ground, µg m ⁻³
HNO3	Concentration of HNO ₃ at ground, µg m ⁻³
NH3	Concentration of NH ₃ at ground, µg m ⁻³
PAN	Concentration of PAN at ground, µg m ⁻³
HNO4	Concentration of HNO ₄ at ground, µg m ⁻³
N2O5	Concentration of N ₂ O ₅ at ground, µg m ⁻³
HONO	Concentration of HONO at ground, µg m ⁻³
ONIT	Concentration of gaseous organic nitrates at ground, µg m ⁻³
O3	Concentration of O ₃ at ground, µg m ⁻³
H2O2	Concentration of H ₂ O ₂ at ground, µg m ⁻³
HCHO	Concentration of formaldehyde at ground, µg m ⁻³
CO	Concentration of CO at ground, µg m ⁻³
ETHE	Concentration of ethene at ground, µg m ⁻³
C5H8	Concentration of isoprene at ground, µg m ⁻³
C10H16	Concentration of monoterpenes at ground, µg m ⁻³
PM2_5_SU	Concentration of PM _{2.5} Sulphate at ground, µg m ⁻³
PM2_5_AM	Concentration of PM _{2.5} Ammonium at ground, µg m ⁻³
PM2_5_NI	Concentration of PM _{2.5} Nitrate at ground, µg m ⁻³
PM2_5_POA	Concentration of PM _{2.5} Primary Organic Aerosol at ground, µg m ⁻³
PM2_5_SOA	Concentration of PM _{2.5} Secondary Organic Aerosol at ground, µg m ⁻³
PM2_5_OC	Concentration of PM _{2.5} Organic Carbon at ground, µg m ⁻³
PM2_5_EC	Concentration of PM _{2.5} Elemental Carbon (Black Carbon) at ground, µg m ⁻³
PM2_5_SS	Concentration of PM _{2.5} Sea Salt at ground, µg m ⁻³
PM2_5_CA	Concentration of PM _{2.5} Calcium at ground, µg m ⁻³
PM2_5_MG	Concentration of PM _{2.5} Magnesium at ground, µg m ⁻³
PM2_5_NSNA	Concentration of PM _{2.5} Non-Sea-Salt Sodium at ground, µg m ⁻³
PM2_5_PK	Concentration of PM _{2.5} Potassium at ground, µg m ⁻³
PM2_5_FE	Concentration of PM _{2.5} Iron at ground, µg m ⁻³



PM2_5_MN	Concentration of PM _{2.5} Manganese at ground, $\mu\text{g m}^{-3}$
PM2_5_OTH	Concentration of PM _{2.5} Other (all not speciated) at ground, $\mu\text{g m}^{-3}$
PM10_SU	Concentration of PM ₁₀ Sulphate at ground, $\mu\text{g m}^{-3}$
PM10_AM	Concentration of PM ₁₀ Ammonium at ground, $\mu\text{g m}^{-3}$
PM10_NI	Concentration of PM ₁₀ Nitrate at ground, $\mu\text{g m}^{-3}$
PM10_POA	Concentration of PM ₁₀ Primary Organic Aerosol at ground, $\mu\text{g m}^{-3}$
PM10_SOA	Concentration of PM ₁₀ Secondary Organic Aerosol at ground, $\mu\text{g m}^{-3}$
PM10_OC	Concentration of PM ₁₀ Organic Carbon (at ground, $\mu\text{g m}^{-3}$
PM10_EC	Concentration of PM ₁₀ Elemental Carbon (Black Carbon) at ground, $\mu\text{g m}^{-3}$
PM10_SS	Concentration of PM ₁₀ Sea Salt at ground, $\mu\text{g m}^{-3}$
PM10_CA	Concentration of PM ₁₀ Calcium at ground, $\mu\text{g m}^{-3}$
PM10_MG	Concentration of PM ₁₀ Magnesium at ground, $\mu\text{g m}^{-3}$
PM10_NSNA	Concentration of PM ₁₀ Non-Sea-Salt Sodium at ground, $\mu\text{g m}^{-3}$
PM10_PK	Concentration of PM ₁₀ Potassium at ground, $\mu\text{g m}^{-3}$
PM10_FE	Concentration of PM ₁₀ Iron at ground, $\mu\text{g m}^{-3}$
PM10_MN	Concentration of PM ₁₀ Manganese at ground, $\mu\text{g m}^{-3}$
PM10_OTH	Concentration of PM ₁₀ Other (all not speciated) at ground, $\mu\text{g m}^{-3}$
PMTOT_SU	Concentration of PMTOT Sulphate at ground, $\mu\text{g m}^{-3}$
PMTOT_AM	Concentration of PMTOT Ammonium at ground, $\mu\text{g m}^{-3}$
PMTOT_NI	Concentration of PMTOT Nitrate at ground, $\mu\text{g m}^{-3}$
PMTOT_POA	Concentration of PMTOT Primary Organic Aerosol at ground, $\mu\text{g m}^{-3}$
PMTOT_SOA	Concentration of PMTOT Secondary Organic Aerosol at ground, $\mu\text{g m}^{-3}$
PMTOT_OC	Concentration of PMTOT Organic Carbon at ground, $\mu\text{g m}^{-3}$
PMTOT_EC	Concentration of PMTOT Elemental Carbon (Black Carbon) at ground, $\mu\text{g m}^{-3}$
PMTOT_SS	Concentration of PMTOT Sea Salt at ground, $\mu\text{g m}^{-3}$
PMTOT_CA	Concentration of PMTOT Calcium at ground, $\mu\text{g m}^{-3}$
PMTOT_MG	Concentration of PMTOT Magnesium at ground, $\mu\text{g m}^{-3}$
PMTOT_NSNA	Concentration of PMTOT Non-Sea-Salt Sodium at ground, $\mu\text{g m}^{-3}$
PMTOT_PK	Concentration of PMTOT Potassium at ground, $\mu\text{g m}^{-3}$
PMTOT_FE	Concentration of PMTOT Iron at ground, $\mu\text{g m}^{-3}$
PMTOT_MN	Concentration of PMTOT Manganese at ground, $\mu\text{g m}^{-3}$
PMTOT_OTH	Concentration of PMTOT Other (all not speciated) at ground, $\mu\text{g m}^{-3}$
PM2_5	Concentration of PM _{2.5} at ground, $\mu\text{g m}^{-3}$
PM2_5N	Number concentration of PM _{2.5} at ground, cm^{-3}
PM10	Concentration of PM ₁₀ at ground, $\mu\text{g m}^{-3}$
PM10N	Number concentration of PM ₁₀ at ground, cm^{-3}



PMTOT	Concentration of total PM at ground, $\mu\text{g m}^{-3}$
PMTOTN	Number concentration of total PM at ground, cm^{-3}
JNO2	Photolysis rate of NO_2 at ground, $1\text{E-}3 \text{ s}^{-1}$
E_SO2	Accumulated emission of SO_2 , kg km^{-2}
E_ANOX	Accumulated emission of anthropogenic $\text{NO}+\text{NO}_2$ as NO_2 , kg km^{-2}
E_NH3	Accumulated emission of NH_3 , kg km^{-2}
E_CO	Accumulated emission of CO , kg km^{-2}
E_PM2_5	Accumulated emission of primary $\text{PM}_{2.5}$, kg km^{-2}
E_PM10	Accumulated emission of primary PM_{10} , kg km^{-2}
E_ETHE	Accumulated emission of ethene, kg-C km^{-2}
E_TOLU	Accumulated emission of toluene, kg-C km^{-2}
E_HCHO	Accumulated emission of formaldehyde, kg-C km^{-2}
E_C5H8	Accumulated emission of isoprene, kg-C km^{-2}
E_MNTP	Accumulated emission of monoterpenes, kg-C km^{-2}
E_SQTP	Accumulated emission of sesquiterpenes, kg-C km^{-2}
E_OVOC	Accumulated emission other VOCs not in above groups, kg-C km^{-2}
E_SNOX	Accumulated emission of soil $\text{NO}+\text{NO}_2$ as NO_2 , kg km^{-2}
E_SS	Accumulated emission of sea salt (all particle sizes), kg km^{-2}
E_WBDUST	Accumulated emission of wind blown dust (all particle sizes), kg km^{-2}
PM2_5_WAT	Concentration of $\text{PM}_{2.5}$ water at ground (if calculated), $\mu\text{g m}^{-3}$
PM10_WAT	Concentration of PM_{10} water at ground (if calculated), $\mu\text{g m}^{-3}$
PMTOT_WAT	Concentration of PMTOT water at ground (if calculated), $\mu\text{g m}^{-3}$

776

777



778 **Table A3. AQMEII4 – Deposition Fluxes (grid)**

779

WFLUX-HSO3-	Wet deposition flux of HSO_3^- ion, eq ha^{-1}
WFLUX-SO4=	Wet deposition flux of $\text{SO}_4^{=}$ ion, eq ha^{-1}
WFLUX-NO3-	Wet deposition flux of NO_3^- ion, eq ha^{-1}
WFLUX-NH4+	Wet deposition flux of NH_4^+ ion, eq ha^{-1}
WFLUX-BCT1	Wet deposition flux of base cations, eq ha^{-1}
WFLUX-TOC	Wet deposition flux of total organic carbon, g ha^{-1}
PRECIP	Surface precipitation, cm
DFLUX-SO2	Dry deposition flux of sulphur dioxide gas, eq ha^{-1}
DFLUX-NO2	Dry deposition flux of nitrogen dioxide gas, eq ha^{-1}
DFLUX-NO	Dry deposition flux of nitrogen monoxide gas, eq ha^{-1}
DFLUX-HNO3	Dry deposition flux of nitric acid gas, eq ha^{-1}
DFLUX-NH3	Net flux of ammonia gas (negative if upwards), eq ha^{-1}
DFLUX-PAN	Dry deposition flux of peroxyacetylnitrate gas, eq ha^{-1}
DFLUX-HNO4	Dry deposition flux of peroxyntic acid gas, eq ha^{-1}
DFLUX-N2O5	Dry deposition flux of dinitrogen pentoxide gas, eq ha^{-1}
DFLUX-ONIT	Dry deposition flux of gaseous organic nitrate, eq ha^{-1}
DFLUX-O3	Dry deposition flux of ozone gas, g ha^{-1}
DFLUX-H2O2	Dry deposition flux of hydrogen peroxide gas, g ha^{-1}
DFLUX-HCHO	Dry deposition flux of formaldehyde gas, g ha^{-1}
DFLUX-P-SO4	Dry deposition flux of total particle sulphate, eq ha^{-1}
DFLUX-P-NO3	Dry deposition flux of total particle nitrate, eq ha^{-1}
DFLUX-P-NH4	Dry deposition flux of total particle ammonium, eq ha^{-1}
DFLUX-P-TC	Dry deposition flux of total particle organic carbon, g ha^{-1}
DFLUX-P-EC	Dry deposition flux of total black carbon, g ha^{-1}
DFLUX-P-BCT1	Dry deposition flux of total particulate base cations, eq ha^{-1}
DFLUX-P-BCT2	Flux of base cat. removed as non-transportable fraction during emissions processing (if available), eq ha^{-1}



DFLUX-P-SS	Dry deposition flux of total sea salt aerosol, moles ha ⁻¹
DFLUX-P-CM	Dry deposition flux of total crustal material (all particulate components not speciated above), g ha ⁻¹
DFLUX-PM2_5	Dry deposition flux of PM _{2.5} , g ha ⁻¹
DFLUX-HONO	Dry deposition flux of HONO, eq ha ⁻¹
RES-AERO	Aerodynamic resistance, s cm ⁻¹

780

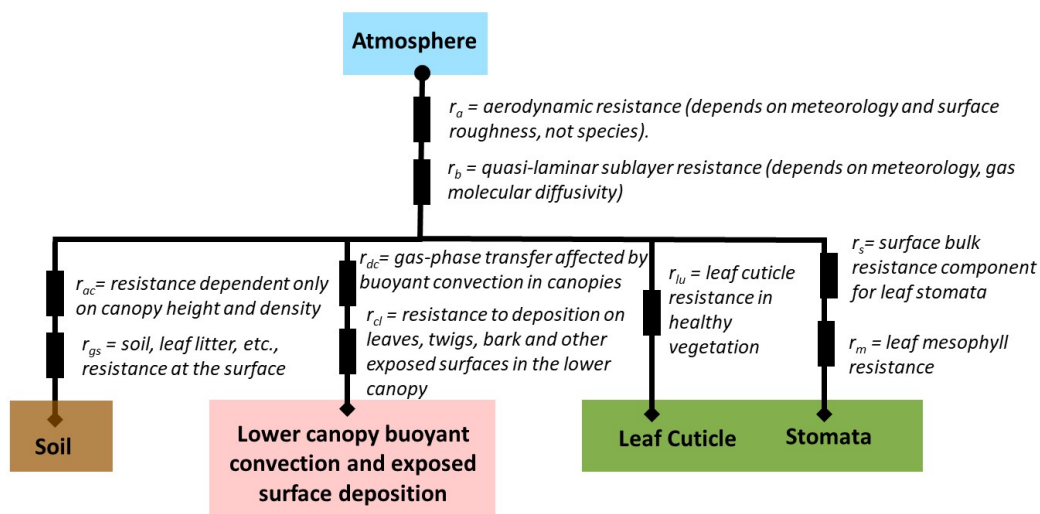


781 **Appendix B: Resistance Diagrams and Calculation of AQMEII4 Reported Dry Deposition Diagnostic Variables for**
 782 **Dry Deposition Schemes Implemented in Participating Models**

783 **Example 1: GEM-MACH model, default Robichaud scheme.**

784 These are the calculations for the Environment and Climate Change Canada model GEM-MACH (Global
 785 Environmental Multiscale- Modelling Air-quality and CHemistry). The resistance diagram for this model is
 786 shown in Figure B1. The deposition algorithm closely follows Wesely’s original hence the similarities to
 787 Figure 1. The scheme includes further modifications incorporating parameterizations from Jarvis (1976),
 788 Val Martin et al. (2014) and other authors; details and references for this scheme may be found in Makar
 789 et al (2018) , Supplemental Information). In GEM-MACH, snow, when present, is treated as a separate
 790 land use type.

791 Figure B1. Resistance diagram for the ECCC GEM-MACH model (default Robichaud scheme).



792

793

794 The main difference between the resistances in Wesely (1989) and the GEM-MACH resistances (aside
 795 from formulation details) is the addition of a surface wetness term, (1-Wst), intended to account for the
 796 influence of wet surfaces on dry deposition.

797

798

799

800

801 Table B1. Example 1: AQMEII4 reported gaseous deposition variables corresponding to the GEM-
 802 MACH/Robichaud resistance model of Figure B1.



Name as described here	AQMEI14 Variable Name	Formulae
r_a	RES-AERO	$RES-AERO = r_a$
r_c	RES-SURF	$RES-SURF = \left((1 - W_{st})(r_s + r_m)^{-1} + (r_{lu})^{-1} + (r_{dc} + r_{cl})^{-1} + (r_{ac} + r_{gs})^{-1} \right)^{-1}$
r_s	RES-STOM	$RES-STOM = r_s$
r_m	RES-MESO	$RES-MESO = r_m$
r_c	RES-CUT	$RES-CUT = r_{lu}$
E_{STOM}	ECOND-ST	$ECOND-ST = \left(\frac{(1 - W_{st})(r_s + r_m)^{-1}}{(1 - W_{st})(r_s + r_m)^{-1} + (r_{lu})^{-1} + (r_{dc} + r_{cl})^{-1} + (r_{ac} + r_{gs})^{-1}} \right) V_d$
E_{CUT}	ECOND-CUT	$ECOND-CUT = \left(\frac{(r_{lu})^{-1}}{(1 - W_{st})(r_s + r_m)^{-1} + (r_{lu})^{-1} + (r_{dc} + r_{cl})^{-1} + (r_{ac} + r_{gs})^{-1}} \right) V_d$
E_{SOIL}	ECOND-SOIL	$ECOND-SOIL = \left(\frac{(r_{dc} + r_{cl})^{-1}}{(1 - W_{st})(r_s + r_m)^{-1} + (r_{lu})^{-1} + (r_{dc} + r_{cl})^{-1} + (r_{ac} + r_{gs})^{-1}} \right) V_d$
E_{LCAN}	ECOND-LCAN	$ECOND-LCAN = \left(\frac{(r_{dc} + r_{cl})^{-1}}{(1 - W_{st})(r_s + r_m)^{-1} + (r_{lu})^{-1} + (r_{dc} + r_{cl})^{-1} + (r_{ac} + r_{gs})^{-1}} \right) V_d$
$r_{b, stom}$	RES-QLST	$RES-QLST = r_b$
$r_{b, cut}$	RES-QLCT	$RES-QLCT = r_b$
$r_{b, soil}$	RES-QLSL	$RES-QLSL = r_b$
$r_{b, lcan}$	RES-QLLC	$RES-QLLC = r_b$
r_{dc}	RES-CONV	$RES-CONV = r_{dc}$

803

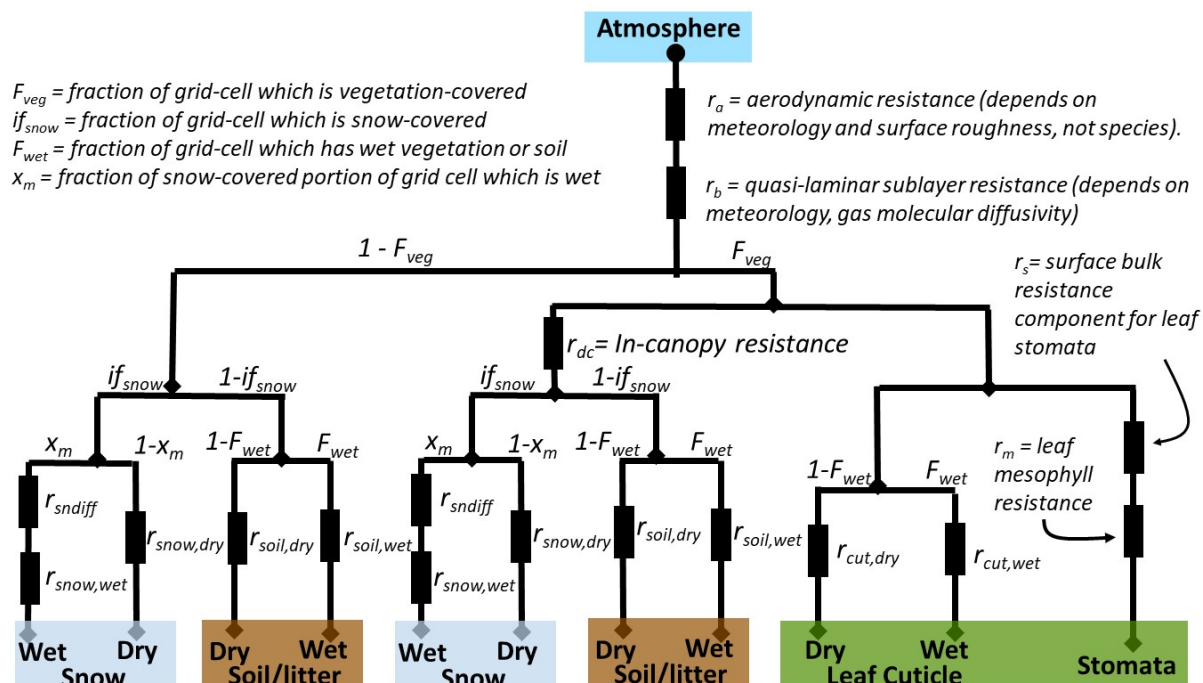
804



805 **Example 2: CMAQ M3DRY.**

806 The second specific air-quality model example is the M3DRY algorithm implemented in the US EPA's
 807 Community Multiscale Air Quality (CMAQ) model, one of two available dry deposition options in that
 808 model. In this particular case, separate branches occur for the vegetated versus non-vegetated fraction
 809 within each model grid cell, and further branching resistance pathways take into account the fraction of
 810 the grid cell which is wet versus dry, and snow-covered versus non-snow covered. In-canopy convective
 811 effects are only calculated for the vegetated fraction.

812 Figure B2. Resistance diagram for the US EPA CMAQ model with the M3DRY deposition option.



813
 814
 815
 816
 817
 818
 819
 820
 821
 822



823

824 Table B2. AQMEI14 reported gaseous deposition variables corresponding to the CMAQ M3DRY resistance
 825 model of Figure B2.

Name as described here	AQMEI14 Name	Variable	Formulae
r_a	RES-AERO		$RES-AERO = r_a$
r_c	RES-SURF		$RES-SURF =$ $\left\{ F_{veg} \left(\frac{1}{r_s + r_m} + \frac{(1-F_{wet})LAI}{r_{cut,dry}} + \frac{F_{wet}LAI}{r_{cut,wet}} + \frac{1}{r_{dc} + \frac{1}{(1-if\ snow) \left(\frac{(1-F_{wet})}{r_{soil,dry}} + \frac{F_{wet}}{r_{soil,wet}} \right) + (if\ snow) \left(\frac{(1-x_m)}{r_{snow,dry}} + \frac{x_m}{r_{sndiff} + r_{snow,wet}} \right)}} \right) \right.$ $\left. + (1 - F_{veg}) \left((1 - if\ snow) \left(\frac{(1-F_{wet})}{r_{soil,dry}} + \frac{F_{wet}}{r_{soil,wet}} \right) + (if\ snow) \left(\frac{(1-x_m)}{r_{snow,dry}} + \frac{x_m}{r_{sndiff} + r_{snow,wet}} \right) \right) \right\}^{-1}$
r_s	RES-STOM		$RES-STOM = r_s$
r_m	RES-MESO		$RES-MESO = r_m$
r_c	RES-CUT		$RES-CUT = \left[\left(\frac{(1-F_{wet})LAI}{r_{cut,dry}} + \frac{F_{wet}LAI}{r_{cut,wet}} \right) \right]^{-1}$
E_{STOM}	ECOND-ST		$ECOND-ST = \left[\frac{F_{veg}}{r_s + r_m} \right] (RES - SURF) V_d$
E_{CUT}	ECOND-CUT		$ECOND-CUT = (RES - CUT)^{-1} (RES - SURF) V_d$
E_{SOIL}	ECOND-SOIL		$ECOND-SOIL = \left[(1 - F_{veg}) \left((1 - if\ snow) \left(\frac{(1-F_{wet})}{r_{soil,dry}} + \frac{F_{wet}}{r_{soil,wet}} \right) + (if\ snow) \left(\frac{(1-x_m)}{r_{snow,dry}} + \frac{x_m}{r_{sndiff} + r_{snow,wet}} \right) \right) \right] (RES - SURF) V_d$
E_{LCAN}	ECOND-LCAN		$ECOND-LCAN = \left[\frac{F_{veg}}{r_{dc} + \frac{1}{(1 - if\ snow) \left(\frac{(1-F_{wet})}{r_{soil,dry}} + \frac{F_{wet}}{r_{soil,wet}} \right) + (if\ snow) \left(\frac{(1-x_m)}{r_{snow,dry}} + \frac{x_m}{r_{sndiff} + r_{snow,wet}} \right)}} \right] (RES - SURF) V_d$
$r_{b, stom}$	RES-QLST		$RES-QLST = r_b$
$r_{b, cut}$	RES-QLCT		$RES-QLCT = r_b$
$r_{b, soil}$	RES-QLSL		$RES-QLSL = r_b$
$r_{b, lcan}$	RES-QLLC		$RES-QLLC = r_b$
r_{dc}	RES-CONV		$RES-CONV = r_{dc}$

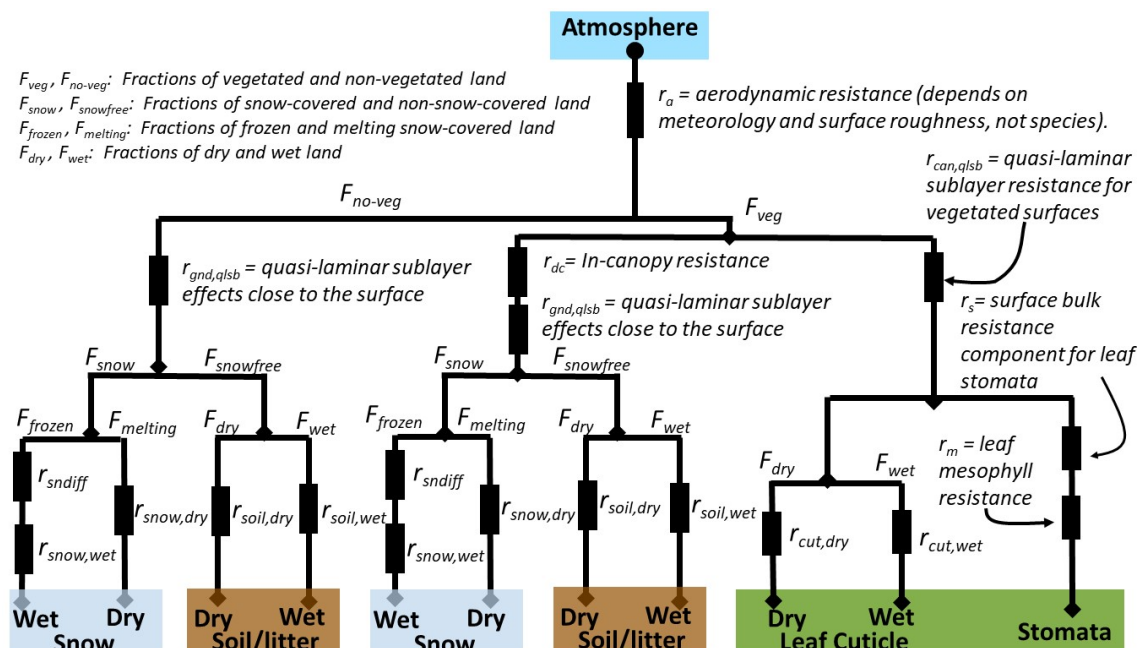
826 Note that the vegetated fraction and leaf area index used in the above equations for CMAQ with the M3DRY
 827 deposition option is for specific LULC types: the quantities in Table B2 will be reported for each of the 16 generic
 828 LULC categories for AQMEI14. Note that the lower canopy pathway has been identified as such due to the presence
 829 of the r_{dc} term; i.e. this points to its similarity with Wesely's original lower canopy pathway.



830 **Example 3: CMAQ STAGE.**

831 The third specific air-quality model example is the algorithm used by the US EPA's Community Multiscale
 832 Air Quality (CMAQ) model with the Surface Tiled Aerosol and Gaseous Exchange (STAGE) deposition
 833 option. In this particular case, separate branches occur for the vegetated versus non-vegetated fraction
 834 for each LULC type within each model grid cell, and further branching resistance pathways take into
 835 account the fraction of the grid cell which is wet versus dry, and snow-covered versus non-snow covered.
 836 In-canopy convective effects are only calculated for in the vegetated fraction.

837 Figure B3. Resistance diagram for the US EPA CMAQ model with the STAGE deposition option. Note, that
 838 this is an extension of the Massad et al. 2010 and Nemitz et al. 2001 resistance model in the CMAQ
 839 modeling framework.



840
 841
 842
 843
 844
 845
 846
 847
 848
 849



850 Table B3. AQMEI14 reported gaseous deposition variables corresponding to the CMAQ STAGE resistance
 851 model of Figure B3.

Name as described here	AQMEI14 Variable Name	Formulae
r_a	RES-AERO	$RES-AERO = r_a$
r_c	RES-SURF	$RES-SURF = \left((r_{can,qlsb} + ((r_s + r_m)^{-1} + (r_{cut})^{-1})^{-1})^{-1} + (r_{dc} + r_{gnd,qlsb} + r_{soil})^{-1} \right)^{-1}$
r_s	RES-STOM	$RES-STOM = r_s$
r_m	RES-MESO	$RES-MESO = r_m$
r_c	RES-CUT	$RES-CUT = r_{cut}$
E_{STOM}	ECOND-ST	$ECOND-ST = \left[\frac{F_{veg}}{r_s + r_m} \right] (RES - SURF) V_d$
E_{CUT}	ECOND-CUT	$ECOND-CUT = \left[\frac{F_{veg}}{r_{cut}} \right] (RES - SURF) V_d$
E_{SOIL}	ECOND-SOIL	$ECOND-SOIL = \left[\frac{F_{no\ veg}}{r_{gnd,qlsb} + r_{soil}} \right] (RES - SURF) V_d$
E_{LCAN}	ECOND-LCAN	$ECOND-LCAN = \left[\frac{F_{veg}}{r_{dc} + r_{gnd,qlsb} + r_{soil} r_{dc} + \frac{1}{r_{soil}}} \right] (RES - SURF) V_d$
$r_{b, stom}$	RES-QLST	$RES-QLST = r_{can,qlsb}$
$r_{b, cut}$	RES-QLCT	$RES-QLCT = r_{can,qlsb}$
$r_{b, soil}$	RES-QLSL	$RES-QLSL = r_{gnd,qlsb}$
$r_{b, lcan}$	RES-QLLC	$RES-QLLC = r_{gnd,qlsb}$
r_{dc}	RES-CONV	$RES-CONV = r_{dc}$

852 Where

853 $F_{veg} + F_{no\ veg} = 1$ Vegetation coverage fractions

854 $F_{snow} + F_{snow\ free} = 1$ Snow coverage fraction

855 $F_{wet} + F_{dry} = 1$ Surface wetness fractions

856 $F_{frozen} + F_{melting} = 1$ Snow melt fractions

857 $r_{cut} = \left(LAI \left(\frac{F_{dry}}{r_{cut, dry}} + \frac{F_{wet}}{r_{cut, wet}} \right) \right)^{-1}$

858 $r_{soil} = \left(F_{no\ snow} \left(\frac{F_{dry}}{r_{soil, dry}} + \frac{F_{wet}}{r_{soil, wet}} \right) + F_{snow} \left(\frac{F_{frozen}}{r_{snow, dry}} + \frac{F_{melting}}{r_{snow, wet}} \right) \right)^{-1}$

859 Note that the vegetated fraction and leaf area index used in the above equations for CMAQ with the STAGE
 860 deposition option is for specific LULC types: the quantities in Table B3 will be reported for each of the 16 generic
 861 LULC categories for AQMEI14. Note that the lower canopy pathway has been identified as such due to the presence
 862 of the r_{dc} term; i.e. this points to its similarity with Wesely's original lower canopy pathway.

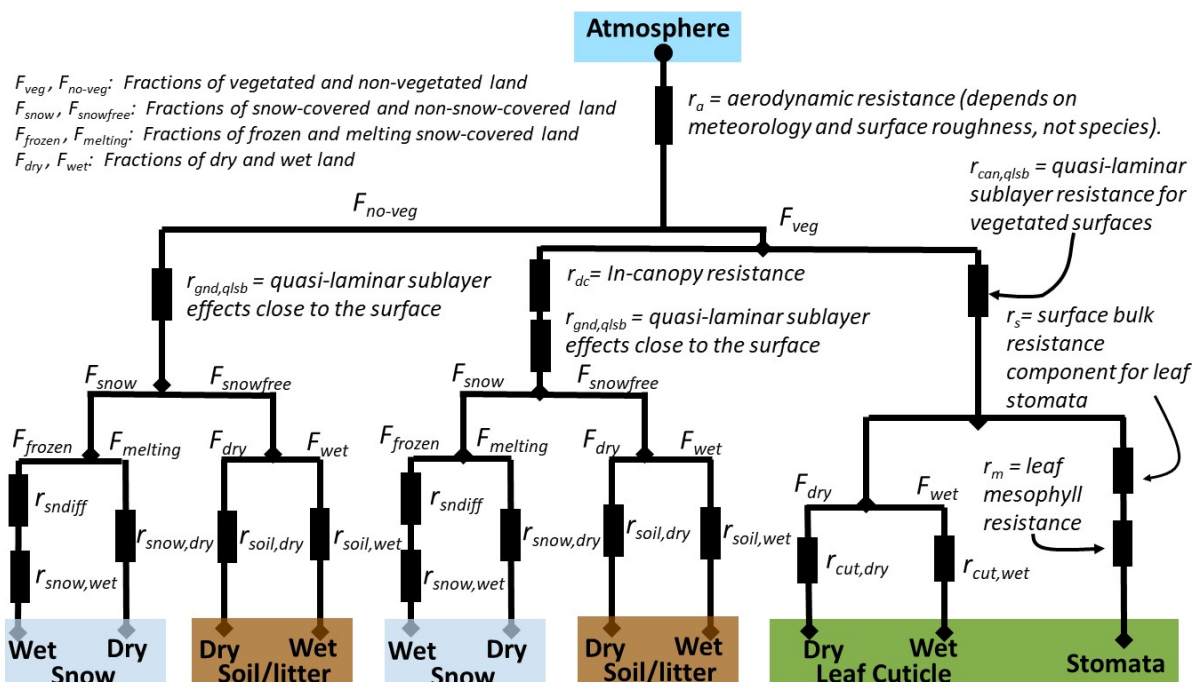
863

864



865 **Example 4. LOTOS EUROS**

866 Figure B4. Resistance diagram for the dry deposition scheme implemented in LOTOS EUROS



867
 868
 869
 870
 871
 872
 873
 874
 875
 876
 877
 878

879 Table B4. AQMEII4 reported gaseous deposition variables corresponding to the LOTOS-EUROS resistance
 880 model of Figure B4



Name as described here	AQMEII4 Variable Name	Description	Formulae
R_a	RES_AERO	Aerodynamic resistance	$\mathbf{RES_AERO} = \frac{\ln\left(\frac{z_r}{z_0}\right) + 4.7 \left(\frac{z_r - z_0}{L}\right)}{\kappa \cdot u^*}$ for stable conditions, κ : von Karman constant (here 0.35), L : Monin-Obukhov length, z_r : reference height, z_0 : height of surface roughness
R_b	RES_QLSB	Quasi-laminar sublayer resistance	$\mathbf{RES_QLSB} = 1.3 \cdot 150 \cdot \sqrt{\frac{L_d}{V(h)}}$ L_d : cross-wind lead dimension, $V(h)$: wind speed at canopy top h , factor 1.3 accounts for differences in diffusivity between heat and ozone
R_c	RES_SURF	Net canopy resistance	$\mathbf{RES_SURF} = \left(\frac{1}{R_w} + \frac{1}{R_{inc} + R_{soil}} + \frac{1}{R_s}\right)^{-1}$ for NO ₂ , NH ₃ , SO ₂ , O ₃ $\mathbf{RES_SURF} = 10$; $\mathbf{RES_SURF} = 50$ (wet conditions) for HNO ₃ , N ₂ O ₅ , NO ₃ , H ₂ O ₂ $\mathbf{RES_SURF} = 2000$ (wet condition); $\mathbf{RES_SURF} = 500 - 70$ (snow condition); $\mathbf{RES_surf} = 9999$ (other conditions) for NO, CO
R_w	RES_CUT	Net cuticle resistance	$\mathbf{RES_CUT} = 2000$ for NO ₂ $\mathbf{RES_CUT} = 2500$ for O ₃ $\mathbf{RES_CUT} = 25000 \cdot e^{(-0.0693+rh)}$ for SO ₂ if rh < 81.3 $\mathbf{RES_CUT} = 5.8 \cdot 10^{11} \cdot e^{(-0.278+rh)}$ for SO ₂ if rh > 81.3 $\mathbf{RES_CUT} = \mathbf{SAI} \cdot \mathbf{a} \cdot e^{(100-RH)/\beta}$ for NH ₃ \mathbf{SAI} : surface area index, $\mathbf{a}=2$ s/m, $\mathbf{\beta}=12$, \mathbf{RH} : relative humidity (%)
R_{inc}		In canopy resistance	$\mathbf{RES_LCAN} = \frac{b \cdot h \cdot \mathbf{SAI}}{u^*}$ b : empirical constant (14 m ⁻¹), h : height of vegetation (m), \mathbf{SAI} : surface area index, u^* : friction velocity (m s ⁻¹)
R_{soil}	RES_SOIL	Soil resistance	Parametrized, frozen soil, wet soil, dry soil $\mathbf{RES_SOIL_FROZEN}=1000$ s m ⁻¹ for NH ₃ ; 2000 s m ⁻¹ for O ₃ , NO ₂ ; 500 s m ⁻¹ for SO ₂ $\mathbf{RES_SOIL_WET} = 10$ s m ⁻¹ for NH ₃ , SO ₂ ; 2000 s m ⁻¹ for O ₃ , NO ₂ $\mathbf{RES_SOIL_DRY}$ (landuse dependent) 200-2000 s m ⁻¹ for O ₃ ; 10-100 s m ⁻¹ for NH ₃ ; 10-1000 s m ⁻¹ for SO ₂ ; 1000-2000 s m ⁻¹ for NO ₂
R_s	RES_STOM	Net stomatal resistance	$\mathbf{RES_STOM} = \frac{1}{E_{stom}}$
E_{STOM}	ECOND_ST	Effective conductance associated with deposition to plant stomata	$\mathbf{ECOND_ST} = \mathbf{EMax}_{stom} \cdot \mathbf{F}_{light} \cdot \mathbf{F}_{phen} \cdot \mathbf{F}_{temp} \cdot \mathbf{F}_{vpd} \cdot \mathbf{F}_{swp} \cdot \mathbf{C}_{diff}$ \mathbf{EMax} : Maximum stomatal conductance (derived for ozone, landuse dependent) \mathbf{F}_{light} , \mathbf{F}_{phen} , \mathbf{F}_{temp} , \mathbf{F}_{vpd} , \mathbf{F}_{swp} : Factors [0-1] for conductance dependency of light, phenology, temperature, vapour pressure and soil-water \mathbf{C}_{diff} : Diffusion coefficient for species with respect to ozone Mesophyll conductance part incorporated in Stomatal conductance



<i>C_{comp}</i>		Bidirectional fluxes of NH ₃	Use of compensation point to derive bi-directional flux for NH ₃ following: Wichink Kruit et al, Modeling the distribution of ammonia across Europe including bi-directional surface–atmosphere exchange. https://doi.org/10.5194/bg-9-5261-2012
-------------------------	--	---	--

881

882

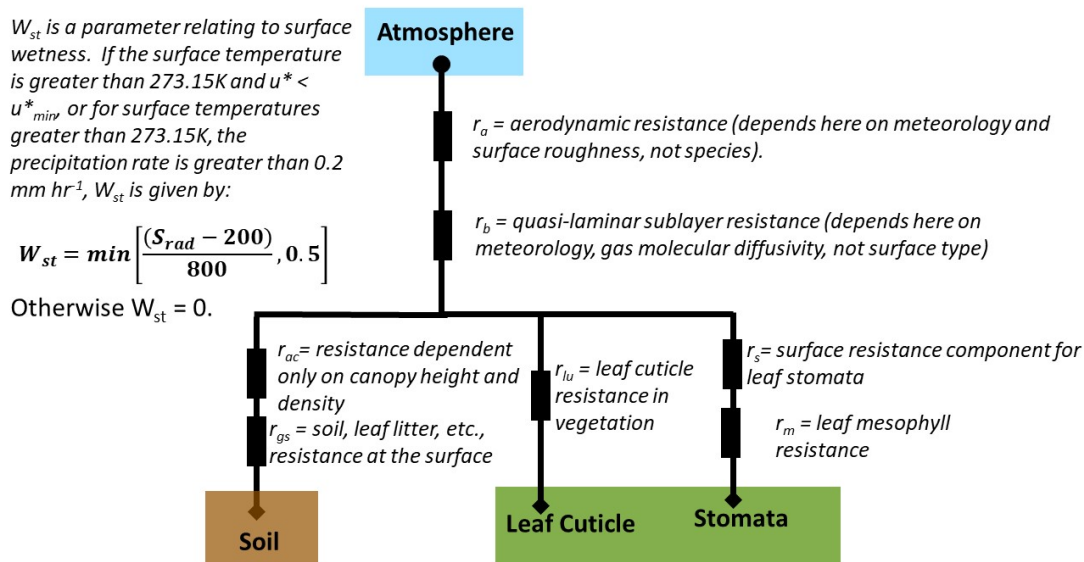
883



884 **Example 5: GEM-MACH model, Zhang scheme.**

885 These are the calculations for the Environment and Climate Change Canada model GEM-MACH (Global
 886 Environmental Multiscale- Modelling Air-quality and CHemistry), using the scheme of Zhang et al (2003,
 887 2010). The resistance diagram for this model is shown in Figure B5.

888 Figure B5. Resistance diagram for the ECCC GEM-MACH model (Zhang scheme).



889

890 The main difference in the overall construction of the deposition scheme relative to the default Robichaud
 891 scheme (aside from the details of how the different terms are calculated) is in the absence of the lower
 892 canopy buoyant convection and exposed surface deposition branch of Wesely's original model. The
 893 details of the parameterizations for the terms in the equations also differ from the Robichaud scheme.

894

895

896 Table B5. AQMEI14 reported gaseous deposition variables corresponding to the GEM-MACH/Zhang
 897 resistance model of Figure B5.

Name as described here	AQMEI14 Variable Name	Formulae
r_a	RES-AERO	$RES-AERO = r_a$
r_c	RES-SURF	$RES-SURF = \left((1 - W_{st})(r_s + r_m)^{-1} + (r_{lu})^{-1} + (r_{ac} + r_{gs})^{-1} \right)^{-1}$
r_s	RES-STOM	$RES-STOM = r_s$
r_m	RES-MESO	$RES-MESO = r_m$
r_c	RES-CUT	$RES-CUT = r_{lu}$



E_{STOM}	ECOND-ST	$ECOND-ST = \left(\frac{(1-W_{st})(r_s+r_m)^{-1}}{(1-W_{st})(r_s+r_m)^{-1}+(r_{lu})^{-1}+(r_{ac}+r_{gs})^{-1}} \right) V_d$
E_{CUT}	ECOND-CUT	$ECOND-CUT = \left(\frac{(r_{lu})^{-1}}{(1-W_{st})(r_s+r_m)^{-1}+(r_{lu})^{-1}+(r_{ac}+r_{gs})^{-1}} \right) V_d$
E_{SOIL}	ECOND-SOIL	$ECOND-SOIL = \left(\frac{(r_{dc}+r_{cl})^{-1}}{(1-W_{st})(r_s+r_m)^{-1}+(r_{lu})^{-1}+(r_{ac}+r_{gs})^{-1}} \right) V_d$
E_{LCAN}	ECOND-LCAN	$ECOND-LCAN = -9$
$r_{b, stom}$	RES-QLST	$RES-QLST = r_b$
$r_{b, cut}$	RES-QLCT	$RES-QLCT = r_b$
$r_{b, soil}$	RES-QLSL	$RES-QLSL = r_b$
$r_{b, lcan}$	RES-QLLC	$RES-QLLC = r_b$
r_{dc}	RES-CONV	$RES-CONV = -9$

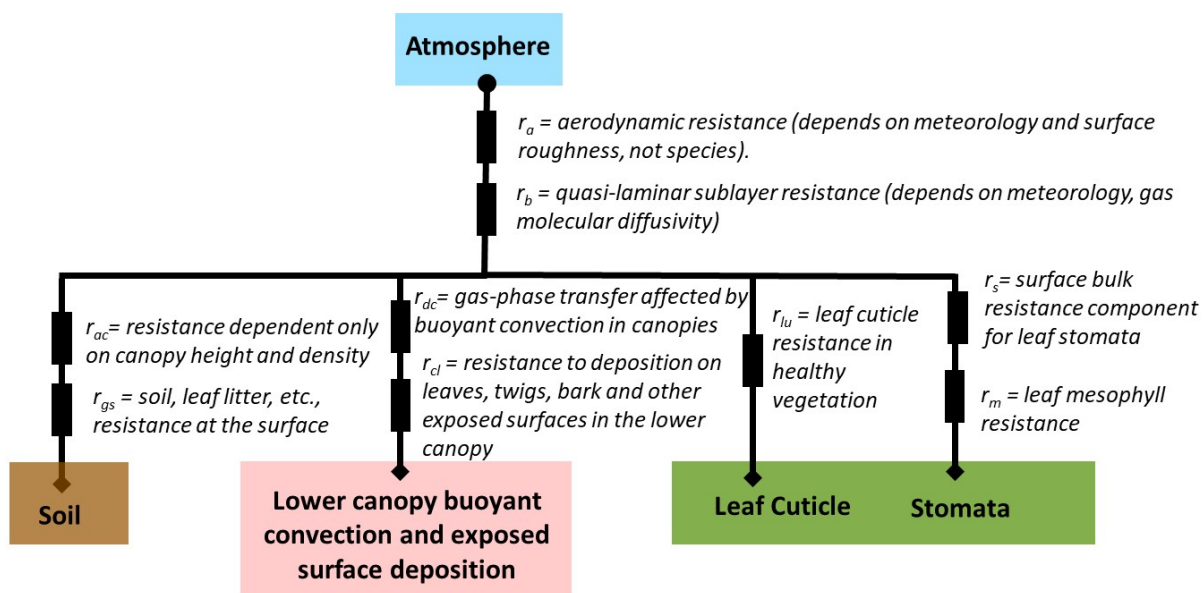
898

899



900 **Example 6. WRF-Chem**

901 Figure B6. Resistance diagram for the gaseous dry deposition scheme implemented in WRF-Chem



902

903 Table B6. AQMEI14 reported gaseous deposition variables corresponding to the WRF-Chem resistance model of
 904 Figure B6.

905

906



Name	AQMEII4 Name	Description	Formula
V_d	VD	Deposition velocity	$V_d = \frac{1}{r_a + r_b + r_c}$
r_a	RES-AERO	Aerodynamic resistance	$\text{Stable: } r_a = \frac{0.74 \ln\left(\frac{z}{z_0}\right) + 4.7 \frac{z - z_0}{L}}{ku^*} \quad z = 2m.$ $\text{Neutral: } r_a = \frac{0.74 \ln\left(\frac{z}{z_0}\right)}{ku^*} \quad z = 2m.$ $\text{Unstable: } r_a = \frac{0.74}{ku^*} \left\{ \ln \left[\frac{\sqrt{1 - 9 \frac{z}{L}} - 1}{\sqrt{1 - 9 \frac{z}{L}} + 1} \right] - \ln \left[\frac{\sqrt{1 - 9 \frac{z_0}{L}} - 1}{\sqrt{1 - 9 \frac{z_0}{L}} + 1} \right] \right\}$
r_c	RES-SURF	Bulk surface resistance	$r_c = \frac{1}{\frac{1}{r_m + r_s} + \frac{1}{r_{cut}} + \frac{1}{r_{dc} + r_{cl}} + \frac{1}{r_{ac} + r_{gs}}}$
r_s	RES-STOM	Net stomatal resistance	$r_s = r_i \left\{ 1 + \left(\frac{200}{Rad + 0.1} \right)^2 \right\} \frac{400}{T(40 - T)}$
r_m	RES-MESO	Net mesophyll resistance	$r_m = \frac{1}{\frac{H}{3000} + 100f_i}$
r_{cut}	RES-CUT	Net cuticle resistance	$r_{cut} = r_{lu}$
E_{STOM}	ECOND-ST	Effective conductance associated with deposition to plant stomata	$E_{STOM} = \frac{1}{r_m + r_s} r_c V_d$
E_{cut}	ECOND-CUT	Effective conductance associated with deposition to plant cuticles	$E_{cut} = \frac{1}{r_{cut}} r_c V_d$
E_{soil}	ECOND-SOIL	Effective conductance associated with deposition to soil and un-vegetated surfaces	$E_{soil} = \frac{1}{r_{ac} + r_{gs}} r_c V_d$



r_{LCAN}	ECOND-LCAN	Effective conductance associated with deposition to the lower canopy.	$E_{LCAN} = \frac{1}{r_{dc} + r_{ct}} r_c V_d$
$r_{b, stom}$	RES-QLST	RES_QLST= r_b Quasi-laminar sub-layer resistance	$r_b = 2(ku^*)^{-1}(S_c/P_r)^{2/3}$
$r_{b, cut}$	RES-QLCT	RES_QLCT= r_b Quasi-laminar sub-layer resistance	$r_b = 2(ku^*)^{-1}(S_c/P_r)^{2/3}$
$r_{b, soil}$	RES-QLSL	RES_QLSL= r_b Quasi-laminar sub-layer resistance	$r_b = 2(ku^*)^{-1}(S_c/P_r)^{2/3}$
$r_{b, lcan}$	RES-QLLC	RES_QLLC= r_b Quasi-laminar sub-layer resistance	$r_b = 2(ku^*)^{-1}(S_c/P_r)^{2/3}$
r_{dc}	RES-CONV	Resistance associated with within-canopy convection.	$r_{dc} = 100(1 + \frac{1000}{Rad})$

907

908

909

Prescribed values (Table data) [pollutant, season]
r_{cl} : for exposed surfaces in the lower canopy SO ₂ , O ₃
r_{ac} : for transfer that depends on canopy height and density
r_{gs} : for ground surfaces SO ₂ , O ₃
r_{si} : for stomatal resistance
r_{lu} : for outer surfaces in the upper canopy
H: Henry's law constant
f_i : Reactivity factor



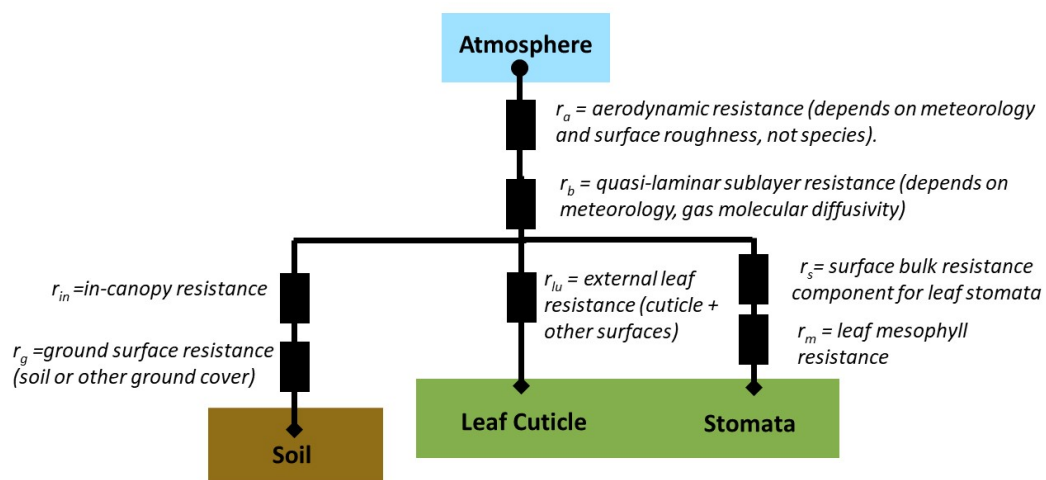
910

911 Example 7: CHIMERE

912

913 Figure B7. Resistance diagram for the dry deposition scheme implemented in CHIMERE

914



915

916

917



918 Table B7: AQMEI4 reported gaseous deposition variables corresponding to the CHIMERE resistance model of Figure
 919 B7

<i>Name as described here</i>	AQMEI4 Variable Name	Formulae
r_a	RES_AERO	$RES_AERO = r_a$
r_b	RES_QLSB	$RES_QLSB = r_b$
r_c	RES_SURF	$RES_SURF = \left((r_s + r_m)^{-1} + (r_{lu})^{-1} + (r_{in} + r_g)^{-1} \right)^{-1}$
r_s	RES_STOM	$RES_STOM = r_s$
r_m	RES_MESO	$RES_MESO = r_m$
r_c	RES_CUT	$RES_CUT = r_{lu}$
E_{STOM}	ECOND_ST	$ECOND_ST = \left(\frac{(r_s + r_m)^{-1}}{(r_s + r_m)^{-1} + (r_{lu})^{-1} + (r_{in} + r_g)^{-1}} \right) V_d$
E_{CUT}	ECOND_CUT	$ECOND_CUT = \left(\frac{(r_{lu})^{-1}}{(r_s + r_m)^{-1} + (r_{lu})^{-1} + (r_{in} + r_g)^{-1}} \right) V_d$
E_{SOIL}	ECONC_SOIL	$ECONC_SOIL = \left(\frac{(r_{in} + r_g)^{-1}}{(r_s + r_m)^{-1} + (r_{lu})^{-1} + (r_{in} + r_g)^{-1}} \right) V_d$
E_{LCAN}	ECONC_LCAN	$ECONC_LCAN = -9$ (not included as a separate deposition pathway)

920



921

922 **Appendix C. Bidirectional Ammonia Fluxes**

923 If a bidirectional flux algorithm for ammonia is employed in the model, then the flux may be either downwards
 924 (defined positive here) or upwards (defined negative, here). The generic equation for the bidirectional flux with this
 925 directionality is:

$$926 \quad F_T = \frac{c_a - c_c}{r_{sum}} \quad (7)$$

927 Where F_T is the net flux, c_a and c_c are the atmospheric and canopy compensation point concentrations of ammonia
 928 gas, and r_{sum} is a sum of resistances. Different sources in the literature make use of different formula for both c_c and
 929 r_{sum} . For example, Zhang et al (2010) employs:

$$930 \quad r_{sum} = r_a + r_b, \text{ and} \quad (8)$$

$$c_c = \frac{\frac{r_a}{r_a + r_b} + \frac{c_s}{r_s} + \frac{c_g}{r_{ac} + r_{gs}}}{(r_a + r_b)^{-1} + (r_s)^{-1} + (r_{ac} + r_{gs})^{-1} + (r_{tu})^{-1}}$$

931 Where c_s and c_g are compensation point concentrations relative to stomata and ground, respectively, and all other
 932 terms are defined as above. CMAQ with the M3dry deposition option uses (Bash et al. 2013, Pleim et al. 2013, Pleim
 933 et al., 2019):

$$934 \quad r_{sum} = r_a + 0.5 r_{inc}$$

$$r_{inc} = 14LAI \frac{h_{can}}{u_*} \text{ (based on Erisman, 1994)} \quad (9)$$

$$c_c = \frac{-B + (B^2 - 4AC)^{0.5}}{2A}$$

935 Where

$$936 \quad A = r_{wet} G_t$$

$$B = r_{wb} G_t + LAI(1 - f_{wet}) - r_{wet} (G_a c_a + G_{sb} c_s + G_g c_g) \quad (10)$$

$$C = -r_{wb} (G_a c_a + G_{sb} c_s + G_g c_g)$$

937 And

$$938 \quad G_a = (r_a + 0.5 r_{inc})^{-1}$$

$$G_{sb} = (r_s + r_b)^{-1}$$

$$G_g = (r_{bg} + 0.5 r_{inc} + r_{soil})^{-1}$$

$$G_t = G_{sb} + G_g + G_a + f_{wet} G_{cw} \quad (11)$$

$$G_{cw} = \frac{LAI}{r_b + r_{wet}}$$

$$r_{wet} = \frac{R_{wo}}{H_{eff}}$$

$$r_{wb} = r_{wet} + LAI [a_h (1 - f_{RH_s}) + r_b]$$

939 Where the terms r_{soil} , H_{eff} , a_h , f_{RH_s} , and R_{wo} are defined in Pleim *et al.* (2013). Note that in the latter reference (their
 940 equation (20)), the summation term in (10) above $G_a c_a$ is repeated twice within the bracketed terms (i.e.
 941 $(G_a c_a + G_{sb} c_s + G_g c_g)$ as above is written $(G_a c_a + G_{sb} c_s + G_a c_a + G_g c_g)$, but this second occurrence of $G_a c_a$ is
 942 likely a typo).

943 CMAQ with the STAGE deposition option closely follows the widely used Massad et al. (2010) and Nemitz et al. (2001)
 944 parameterizations modified to include the option for a cuticular compensation point and employs the same
 945 resistance model for all deposited species as it reduced to RES-SURF from table B3 when the stomatal, C_s , cuticular,
 946 C_{cut} , and ground, C_g , compensation points are zero. NH_3 bidirectional flux from the cuticle has been shown to be
 947 important (cuticular NH_3 reference) however parameterizations applicable in a regional-scale model do not yet exist.



948
$$r_g = r_{dc} + r_{gnd,qlsb} + r_{gs} \quad (12)$$

949
$$r_{sum} = r_a \quad (13)$$

950
$$c_c = \frac{\frac{c_a}{r_a} + \frac{c_{leaf}}{r_{can,qlsb}} + \frac{c_g}{r_g}}{(r_a)^{-1} + (r_{can,qlsb})^{-1} + (r_{dc} + r_{gnd,qlsb} + r_{gs})^{-1}} \quad (14)$$

951

952 c_{leaf} is the leaf compensation point and is estimated by solving for the exchange between the canopy compensation
 953 point and the atmosphere, stomata, cuticle and ground following Kirchhoff's current law (e.g. Nemitz *et al.* 2000).
 954 c_{leaf} is solved from this system of equations as:

955
$$c_{leaf} = \frac{\frac{c_a}{r_a r_{can,qlsb}} + \frac{c_s}{r_a r_s + r_{can,qlsb} r_s + r_g r_s} + \frac{c_{cut}}{r_a r_{cut} + r_{can,qlsb} r_{cut} + r_g r_{cut}} + \frac{c_g}{r_{dc} + r_{gnd,qlsb} + r_{gs}}}{(r_a r_{can,qlsb})^{-1} + (r_a r_s)^{-1} + (r_a r_{cut})^{-1} + (r_{can,qlsb} r_s)^{-1} + (r_{can,qlsb} r_{cut})^{-1} + (r_{can,qlsb} r_g)^{-1} + (r_g r_s)^{-1} + (r_g r_{cut})^{-1}} \quad (15)$$

956

957 The resistances r_{cut} , $r_{can,qlsb}$, and $r_{gnd,qlsb}$ are taken from Massad *et al.* 2010, r_{dc} follows Shuttleworth and Wallace (1985)
 958 but integrated the canopy transport model of Yi 2008 using the in-canopy eddy diffusivity of Bash *et al.* 2010 from
 959 the soil surface to top of the canopy and assuming $r_a = p_r U/u_*^2$, the remainder of the resistances are the same as
 960 CMAQ with the M3dry deposition option.

961
$$r_{dc} = r_a \left(e^{\frac{LAI}{2}} - 1 \right) \quad (16)$$

962

963 Comparing approaches (8 through 16), r_{sum} , r_a , and c_c are held in common, and these approaches also make use of a
 964 stomatal (c_s) and ground (c_g) compensation point concentration, although how these terms are combined varies
 965 considerably between these approaches. For this reason, these common terms are reported as a separate TSD for
 966 ammonia bidirectional fluxes in AQMEI4 in order to allow cross-comparison of different approaches.

967

968 Note that the net flux of ammonia F_T appears as DFLUX-NH3 in the AQMEI4 documentation provided to participants
 969 as TSDs and may be positive or negative depending on direction. Ammonia values for r_b , net canopy resistance,
 970 stomatal resistance, mesophyll resistance, cuticle resistance and the three effective conductances also appear
 971 elsewhere in the TSDs, both for the grid scale and by AQMEI4 LULC category.

972